# Evaluation of binding performance of bioactive compounds against main protease and mutant model spike receptor binding domain of SARS-CoV-2: Docking, ADMET properties and molecular dynamics simulation study

Maheswata Moharana [a,1], Anuradha Das [b,1], Satya Narayan Sahu [c], Subrat Kumar Pattanayak [a,*], Fahmida Khan [a,**]

[a] Department of Chemistry, National Institute of Technology, Raipur, 492010, India
[b] School of Chemical Sciences, National Institute of Science Education and Research, Bhubaneswar, 752050, India
[c] School of Applied Sciences, Kalinga Institute of Industrial Technology (KIIT) Deemed to Be University, Bhubaneswar, 751024, India

## ABSTRACT

Phytochemicals present in medicinal plants have a variety of biological activities that help to combat against diseases. As part of efforts to study the binding performance of different phytochemicals derived from different plants like *Zingiber officinale, Citrus limon, Syzygiumaromaticum, Ocimum tenuiflorum and Curcumin*. We have screened 424 molecules. The binding affinity as well as physicochemical properties of the thebaine, acacetin, indomethacin, crinamineacetate, (S)-1-Piperideine-6-carboxylate, levamisole, melatonin, nicotinicacid, curcumin, methotrimeprazine, omeprazole, and methaqualone phytocompounds were analyzed through computational study. From the molecular docking study we found that, LEU50, ASN72, PRO96, TYR154, GLY170, ALA193, ARG222, and MET274 residues of main protease play a crucial role in binding with ligands. The present study revealed a noticeable interaction of GLY446, SER477, GLY482, THR500 and LEU518 residues with mutant of spike receptor binding domain SARS-CoV-2 protein were observed. Finally, 100 ns molecular dynamics simulation were used to study their dynamic properties as well as conformational flexibility. Free energy landscape analysis was performed of the 6LU7- acacetin and 6Y2E-acacetin systems and spike RBD-acacetin system. From molecular docking study and molecular dynamics study revealed that, the compound acacetin shows promising inhibitor towards both main protease as well as mutant spike RBD of SARS-CoV-2 protein.

## 1. Introduction

Plant-derived compounds are used to treat various diseases [1–4]. Phytochemicals present in medicinal plants have a variety of biological activities that help to fight against many diseases [5,6]. Various plant species have been reported to have promising antiviral activity against viral respiratory infections [7]. In order to find potent therapeutic agents to avoid SARS-CoV-2 infection, recent research has been performed on a number of medicinal plants [8,9]. Secondary metabolites present in medicinal plants may be used as natural antiviral agents to fight COVID-19. Primary metabolites include alkaloids, flavonoids, tannins, terpenes, glycosides, and lignin. A number of diseases have been prevented or treated with drugs derived from bioactive phytocompounds

found in medicinal plants. Antiviral, antimicrobial, antibacterial, anti-parasitic, and anti-inflammatory effects have prompted comprehensive study. Since there are currently only a few medicines available to treat viral diseases, more attention should be paid to the development of phytocompound-based drugs. To find an alternative drug to use as a potential SARS-CoV-2 receptor ACE2 inhibitor, researchers used molecular docking experiments on different phytocompound components present in medicinal plants with the main protease SARS-CoV-2 [10]. The spike protein receptor-binding domain (Spike RBD) is responsible for allowing coronavirus to reach the host cell and being discovered as an antiviral drug target. Some of the bioactive compounds were discovered in medicinal plants using molecular dynamics (MD) simulation and binding energy analysis to block SARS-CoV-2 S-RBD which

binds primarily with the human angiotensin-converting enzyme 2 (ACE2) [11]. Compounds extracted from plants have fewer side effects than chemical/synthetic drugs. An *in-silico* method was used to screen and discover plant-extracted phytocompounds that act as potential inhibitor against the SARS-CoV-2 proteins. Viral replication is caused by the endoribonuclease (NSP15) and protease (3CL pro) proteins. Demethoxy curcumin, bisdemethoxy curcumin, scutellarin, quercetin, and myricetin are plant derived compounds and potential drugs against the main protease (3CL pro) and endoribonuclease (NSP15) proteins of SARS-CoV-2 [12]. A wide range of phytochemicals found in medicinal plants are used to treat different diseases in previously [13,14].

Severe acute respiratory syndrome coronvirus 2 (SARC-CoV-2) a highly infectious virus that has contributed to substantial mortality [15, 16]. The respiratory distress syndrome symptoms caused by coronavirus disease-19 (COVID-19). The respiratory distress syndrome symptoms were found to be similar to those caused by corona viruses that cause extreme severe acute respiratory syndrome (SARS) and Middle East respiratory syndrome (MERS) [17]. The single standard-RNA of corona virus is encapsulated in the membrane and the virion is contained in phosphorylated nucleocapsid protein and RNA [18]. The coronavirus consists of four structural proteins called Spike(S), Envelope(E), Membrane(M), and Nucleocapsid(N). The corona virus genome is encoded with pp1a [19] and pp1b (2020) polyproteins [20]. The mainprotease encoded with open reading frames, also known as 3CLpro (3C-like protease or chymotrypsin-like protease) and PLpro (Papain-like protease), The above-mentioned polyproteins are further cleaved into 16 non-structural proteins (NSPs). These non-structural proteins are attributed to the quality of sub genomic RNAs encoding the four main structural proteins and other accessory proteins [21]. As a result, these proteases, especially Mpro, play a critical role, and regulating Mpro's activity can prevent viral replication within the host [22]. The virus binds to the angiotensin-converting-enzyme-2(ACE2) receptor and enters the host, causing a respiratory tract infection. The existence of the main protease ($M^{pro}$) enzyme in SARS-CoV-2 was recently studied by Liu et al. [23]. SARS-CoV-2 $M^{pro}$ has also been linked to SARS-CoV-2 replication inhibition [24]. Therefore this enzyme may be targeted for drug production. According to some reports [25], promising antiviral drugs have high inhibitory activity and can avoid SARS-CoV-2 infection. COVID-19 is a major problem and research & development of drugs and vaccines to combat it is ongoing. Various antiviral agents such as ritonavir, chloroquine phosphate, arbidol and rabivirin have efficacy against SARS-CoV [26]. FDA-approved drugs have been tested in laboratory trials to see whether they are successful against SARS-CoV-2 [27, 28]. The spike protein forms an N-terminal subunit and a C-terminal membrane proximal subunit [29]. Again these subunits consist of different domain. The receptor-binding domain (RBD) of the SARS-CoV-2 spike protein interacts with the human ACE-2 receptor [30, 31]. It was reported from a recent study [32–35], the infectivity and reactivity towards a panel of neutralizing antibodies and sera from convalescent patients, mutations and glycosylation site modifications have been found in human SARS-CoV-2 spike proteins. The human pathogen SARS-CoV-2 enters into host cell by the help of spike RBD of spike protein binds to the target cell of the host through angiotensin converting enzyme 2 (ACE2) and it causes multiple complications with the host [36]. After it gets mutated in the position L452R and E484Q it increases the binding efficacy with ACE2 of host and these mutations are responsible for second wave in India [37,38].

Antiviral effects have been discovered in herbal solution extracts, as well as anti-diabetic, anti-bacterial, anti-fungal, and antioxidant properties. A GC/MS analysis of herbal solution revealed the presence of several antiviral phytochemicals that can be identified using the NIST database. The efficacy of these selected bioactive molecules against COVID-19 was determined using the molecular docking process. Phytochemicals have been identified using the separation technique. Binding pockets of active sites need a complex configuration to ensure ligand specificity. The surface characteristics properties are needed for precise,

organized, and highly regulated protein binding. Herbal solution containing ginger (Zingiber officinale), honey, lemon (Citrus limon), black pepper (Piper nigrum), turmeric (curcumin), cinnamon(Cinnamomum verum), cloves (Syzygiumaromaticum), and tulsi (Ocimumtenuiflorum) through methanolic extract shows the existence of several bioactive compounds, including alkaloids, steroids, phenols, flavonoids, and terpenoids.

We have screened the phytochemicals present in the herbal solution (medicinal plant extracts). The binding efficacy properties of thebaine, acacetin, indomethacin, crinamine acetate, (S)-1-Piperideine-6-carboxylate,levamisole, melatonin, nicotinic acid, curcumin, methotrimeprazine, omeprazole, and methaqualone with protease proteins as well as mutant spike receptor binding domain protein were analyzed. The detailed study is summarized as follows. In section 2, we discussed computational models and simulation information. Physicochemical properties of phytochemicals are discussed in section 3. The section 3 also discussed about molecular dynamics simulation properties of ligands and section4 summarize our results.

## 2. Materials method and computational details

For protease protein of SARS-CoV-2, we selected the structure of SARS-CoV-2 protease proteins with PDB ID:6LU7 and 6Y2E. For spike receptor binding domain protein we selected the PDB ID: 6W41 ('C'chain). All were collected from the protein data bank (www.rcsb.org). After that, we converted the 'C' chain of 6W41 model into mutant model of spike RBD at the position L452R and E484Q. The plant materials listed in the Table S1 were grinded into small pieces by using mortar and pestle. These were then dissolved in 100 mL of de-ionized water in a 250 mL conical flask. It was then heated for 30 min at 90°C in a hot water bath. The reaction mixture was then filtered using suction filtration (Buchner funnel) and the filtrate was collected. The extract was allowed to cool to room temperature and stored for gas chromatography-mass spectrometry (GCMS) study. From this extract around 500 μL was taken in a 5 mL vial and 500 μL of methanol was added to this and was mixed properly. The sample was then filtered using 0.22 μm syringe filter (Abdos). 1 μL of the sample was injected to the GCMS by Autosampler and the data was recorded. A mechanical grinder was used to grind the plant materials into small pieces. These were then dissolved in 100 mL of water, heated for 15 min at 80°C, and condensed to 5 mL. The extract was then allowed to cool to room temperature before being stored for gas chromatography-mass spectrometry (GC-MS) study. It was carried out with a helium carrier gas on a Thermo Fisher ITQ 900 instrument (EI) and TG-SQC capillary column. RBDThe below mentioned parameters were used in the GC-MS analysis: The oven temperature was steadily increased from 60°C to 300°C at a rate of 15°C/min for a 5-min hold time. The mass range was fixed in between 50 and 650 $m/z$ and the ion source temperature was 220°C.The NIST-MS Library [https://chemdata.nist.gov/] was used to search and identify each component. The details of sample preparation methods were described in supplementary part. Here we studied phytochemicals like thebaine, acacetin, indomethacin, crinamine acetate, (S)-1-Piperideine-6-carboxylate, levamisole, melatonin, nicotinic acid, curcumin, methotrimeprazine, omeprazole, and methaqualone. The structure of above discussed phytochemicals was retrieved from PubChem database (https://pubchem.ncbi.nlm.nih.gov/). For molecular docking study, we removed water molecules and hetero atoms. Polar hydrogen atoms and Kollman charges were added on it through AutoDockTools-1.5.6 (ADT). AutoDock software [39] was used to perform molecular docking [40–42] to determine the binding energy between the proteins and different phytochemicals. The AutoDock vina performs the docking procedure using the Gradient optimization algorithm. We set the grid box to cover the predicted binding pocket present in the protease protein with grid sizes of 90, 90, and 80 in different coordinate directions to start the docking phase. The box spacing with 0.375 Å was maintained for entire system. Center size was adjusted to -4.23, 5.64, -8.97 in x, y and z

**Table 1**
Name of compounds, retention time and biological activity.

| Compound name | Retention time (Minute) | Mass/ Charge (*m/z*) | Biological activity with references |
|---|---|---|---|
| Thebaine | 19.31 | 311 | Antiviral [57] |
| Acacetin | 16.02 | 284 | Antiviral property [58] |
| Indomethacin | 20.57 | 357.03 | Antiviral activity [59] |
| Crinamine acetate | 7.17 | 343 | Antiviral activity [60] |
| (S)-1-Piperideine-6-carboxylate | 18.98 | 126.13 | Antiviral activity [61] |
| Levamisole | 20.55 | 204.29 | Antiviral activity [62] |
| Melatonin | 15.69 | 232.28 | Antiviral activity [63] |
| Nicotinic acid | 14.43 | 123.11 | Antiviral activity [64] |
| Curcumin | 15.48 | 368.4 | Antiviral activity [65] |
| Omeprazole | 18.92 | 354.4 | Antiviral activity [65] |
| Methotrimeprazine | 7.18 | 328 | Antiviral activity [66] |
| Methaqualone | 15.69 | 235 | Antiviral activity [67] |

direction respectively. Similarly for the mutant spike RBD the grid box size of 100, 100, 126 in different coordinate and center size was adjusted to -39.944, -40.736, -6.034 with spacing 0.436Å.All the snapshots were captured with the help of Discovery studio visualization tool [43]. The physiochemical and ADME properties [44] of phytochemicals studied through Swiss ADME (http://www.swissadme.ch). Physiochemical properties such as partition coefficient (Log P), hydrogen bond donors/acceptor, solubility coefficient (LogS), number of rotatable bonds and polar surface area (PSA).

Now we studied the dynamical properties [45–47]. We conducted molecular dynamics simulation analysis using the GROMACS software [48] CHARMM General force field (CGenFF) was used to perform ligand parameterization [49]. Noted, we have used CHARMM General force field [50] for topology file preparation. Three site water model of TIP3P water model was used to solve all of the systems [51]. A total of 19237, 19952, and 13439 water molecules were added to a cubic simulation box containing the 6LU7, 6Y2E, and spike-RBD protein, respectively. Periodic boundary conditions have been used to prevent the edge effect. We applied an appropriate number of counter ions to maintain neutral simulated systems. During the energy minimization method, we used the steepest descent algorithm [52]. Equilibration with position restriction was performed after energy minimization under the NVT (constant number, constant volume, and constant temperature) and NPT (constant

number, constant pressure, and constant temperature) ensembles. In NVT equilibration, the Berendsen thermostat [53] algorithm was employed to keep the system at a constant volume and temperature (300 K). In addition, NPT equilibration was carried out at a constant pressure (1 bar) using the Parrinello-Rahman barostat [54]. LINCS algorithm [55] was employed for all covalent bonds. The Particle Mesh Ewald method was used to manage long-range electrostatic power [56]. A time step of 2 fs has been followed. In the production simulation phase, we used 100ns for all three simulation trajectories separately.

## 3. Result and discussions

The extract of herbal solution contains a total of 424 compounds within the retention time of 22 min. 12 major bioactive compounds were identified given in the Table 1.

### 3.1. Physicochemical properties of phytochemicals

All of the phytocompounds studied had a molecular weight of less than 500 Da. The greater the hydrophobicity ability to reach the plasma membrane of the cell, the higher the Log P value of the molecules absorption parameter or hydrophobicity is expressed. Except for (S)-1-Piperideine-6-carboxylate and nicotinic acid, all other compounds have a Log P value greater than one. The value of the water solubility coefficient, or log S, is an important parameter for studying the pharmacokinetic behaviour of the lead molecule's distribution and absorption. Except (S)-1-Piperideine-6-carboxylatefor all other compounds, the Log S value was limits within -4.5 to -1. The polar surface area (PSA), which is related to absorption, is calculated to be less than 140 Å$^2$. Here, all studied compounds lies within range of polar surface area. The number of rotatable bonds is always less than 10, and the minimum rotatable bond after molecular simulation provides a better proof of the structure. All of the parameters studied above for the above-mentioned phytocompounds (except (S)-1-Piperideine-6-carboxylate and nicotinic acid) were evaluated with Lipinski's rules (Huang, et al. 2014) expressing the drug similarity of and of the phytocompounds. Table 2 displays the expected drug resemblance properties of the phytochemicals tested. The pharmacokinetic properties of gastrointestinal (GI), blood-brain-barrier (BBB), skin permeate (Log Kp) and CYP (CYP1A2, CYP2C19, CYP2C9, CYP2D6, CYP3A4) inhibitors are studied for each of the phytocompounds shown in Table 3. GI determines the amount of drug to be absorbed by the gastrointestinal tract; all phytochemicals are strongly absorbed by the gastrointestinal tract. The ability of phytocompounds to cross the blood-brain barrier is then investigated (BBB). The BBB findings show that none of the phytocompounds tested can cross the blood-brain barrier, meaning that they should be avoided.

**Table 2**
Drug likeness properties of phytochemicals.

| Phytochemical Name | Pubchem Id | Molecular Formula | Mol.weight (g/mol) | TPSA (Å$^2$) | No.of RB | Log P | Log S | HBA | HBD |
|---|---|---|---|---|---|---|---|---|---|
| Thebaine | 5324289 | $C_{19}H_{21}NO_3$ | 311.37 | 30.93 | 2 | 2.47 | −3.22 | 4 | 0 |
| Acacetin | 5280442 | $C_{16}H_{12}O_5$ | 284.26 | 79.90 | 2 | 2.52 | −4.14 | 5 | 2 |
| Indomethacin | 3715 | $C_{19}H_{16}C_lNO_4$ | 357.79 | 68.53 | 5 | 3.63 | −4.86 | 4 | 1 |
| Crinamine acetate | 541205 | $C_{19}H_{21}NO_5$ | 343.37 | 57.23 | 3 | 1.93 | −3.11 | 6 | 0 |
| (S)-1-Piperideine -6-carboxylate | 45266761 | $C_6H_8NO_2$ | 126.13 | 52.49 | 1 | 0.15 | −0.46 | 3 | 0 |
| Levamisole | 26879 | $C_{11}H_{12}N_2S$ | 204.29 | 40.90 | 1 | 1.96 | −2.52 | 1 | 1 |
| Melatonin | 896 | $C_{13}H_{16}N_2O_2$ | 232.28 | 54.12 | 5 | 1.83 | −2.34 | 2 | 2 |
| Nicotinic acid | 938 | $C_6H_5NO_2$ | 123.11 | 50.19 | 1 | 0.32 | −1.26 | 3 | 1 |
| Curcumin | 969516 | $C_{21}H_{20}O_6$ | 368.38 | 93.06 | 8 | 3.03 | −3.94 | 6 | 2 |
| Methotrimeprazine | 72287 | $C_{19}H_{24}N_2OS$ | 328.47 | 41.01 | 5 | 3.93 | −4.88 | 2 | 0 |
| Omeprazole | 4594 | $C_{17}H_{19}N_3O_3S$ | 345.42 | 96.31 | 5 | 2.31 | −3.52 | 5 | 1 |
| Methaqualone | 6292 | $C_{16}H_{14}N_2O$ | 250.30 | 34.89 | 1 | 2.96 | −3.52 | 2 | 0 |

**Table 3**
Predicted pharmacokinetic properties of studied phytochemicals.

| Molecule Name | GI Absorption | Log $K_p$ in cm/s | BBB permeant | CYP1A2 inhibitor | CYP2C19 inhibitor | CYP2C9 inhibitor | CYP2D6 inhibitor | CYP3A4 inhibitor |
|---|---|---|---|---|---|---|---|---|
| Thebaine | High | −6.64 | Yes | Yes | No | No | Yes | Yes |
| Acacetin | High | −5.66 | No | Yes | No | Yes | Yes | Yes |
| Indomethacin | High | −5.45 | Yes | Yes | Yes | Yes | No | No |
| Crinamine acetate | High | −7.09 | Yes | No | No | No | Yes | No |
| (S)-1-Piperideine-6-carboxylate | High | −7.18 | No | No | No | No | No | No |
| Levamisole | High | −6.24 | Yes | No | No | No | No | No |
| Melatonin | High | −6.59 | Yes | Yes | No | No | No | No |
| Nicotinic acid | High | −6.80 | Yes | No | No | No | No | No |
| Curcumin | High | −6.28 | No | No | No | Yes | No | Yes |
| Methotrimeprazine | High | −4.98 | Yes | Yes | No | Yes | Yes | No |
| Omeprazole | High | −6.82 | No | Yes | Yes | No | Yes | Yes |
| Methaqualone | High | −6.05 | Yes | Yes | Yes | No | No | No |
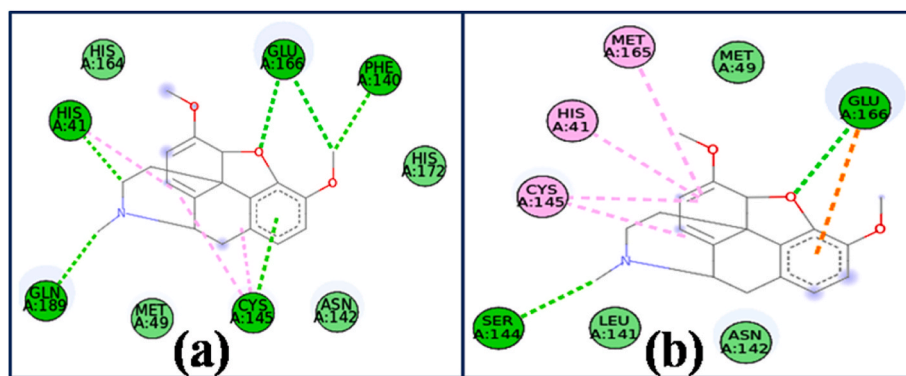


**Fig. 1.** Molecular interactions of Thebaine with (a) 6LU7 and (b) 6Y2E proteins. Hydrophobic interaction is represented by violet and pink dotted bonds, hydrogen bonds are represented by green dotted bonds, and electrostatic interaction is represented by a deep yellow dotted bond. (For interpretation of the references to color in this figure legend, the reader is referred to the Web version of this article.)
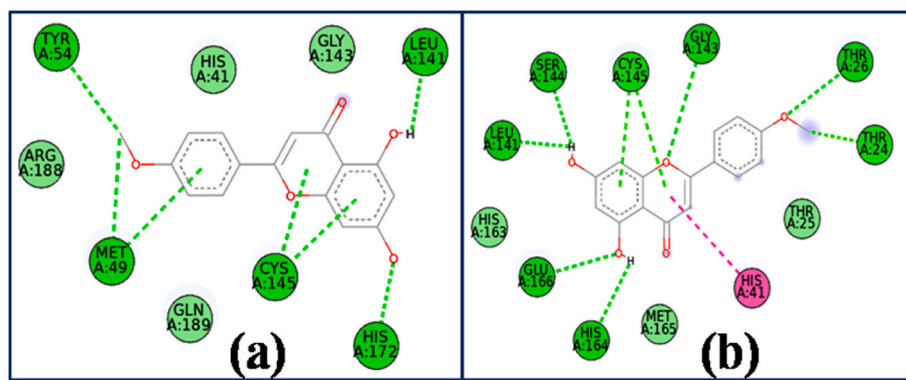


**Fig. 2.** Molecular interactions of Acacetin with (a) 6LU7 and (b) 6Y2E proteins. Hydrophobic interaction is represented by violet and pink dotted bonds, hydrogen bonds are represented by green dotted bonds, and electrostatic interaction is represented by a deep yellow dotted bond. (For interpretation of the references to color in this figure legend, the reader is referred to the Web version of this article.)

### 3.2. Molecular docking

Protein 6LU7 has a binding energy of -6.93 kcal/mol with the compound thebaine. Hydrogen bonding was observed in GLU 166, HIS 41, GLN189, PHE140, and GLU 166 residues. The ligand's C-atom is in H-bonding contact with the residues MET49, TYR54, and CYS145, and the form of the interaction is C–H interaction and pi-donor hydrogen bonding interaction, with bond lengths ranging from 3.08 to 3.90 Å. With a bond length of 4.31, the amino acid residue MET49 made hydrophobic contact with the ligand. Fig. 1(a) depicts a schematic diagram of the above relationship. Thebaine-protease protein 6Y2E, has a binding energy of -7.28 kcal/mol. GLU 166 and SER 144 are linked with the ligand by hydrogen bonding with bond length ranging from 2.97 to 2.84 Å. GLU 166 residue is involved in electrostatic interaction with bond length 4.40 Å and CYS145, HIS41, MET165 involved in hydrophobic interaction with bond length 4.48 to 5.40 Å. The binding mode interaction is shown in the schematic Fig. 1 (b).

With compound acacetin, the protease protein binding energy was estimated to be -7.77 kcal/mol. The ligand's H and O atoms form traditional H-bonds with the amino acid residues LEU141, HIS172, and MET49, with bond lengths of 1.66 and 3.76 Å. The H-bonding interaction between the ligand and the residues MET49, TYR54, and CYS145 is
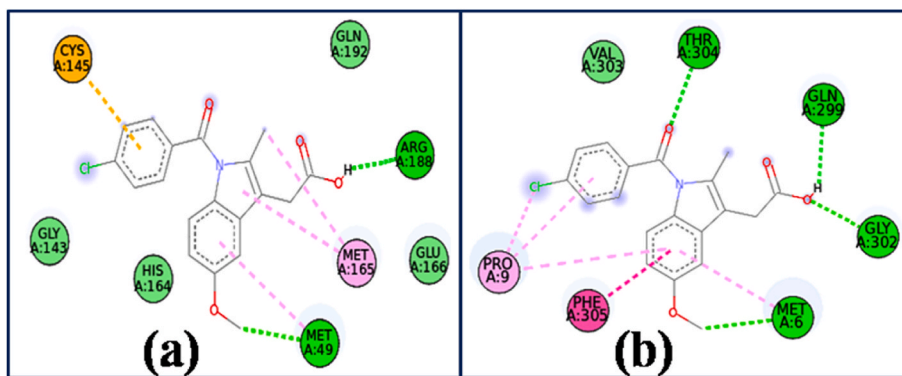
**Fig. 3.** Schematic diagram of Indomethacin interacts with (a) 6LU7 and (b) 6Y2E at the molecular level. Hydrophobic interaction is defined by violet and pink dotted bonds, hydrogen bonds by green dotted bonds, and electrostatic interaction by deep yellow dotted bonds. (For interpretation of the references to color in this figure legend, the reader is referred to the Web version of this article.)
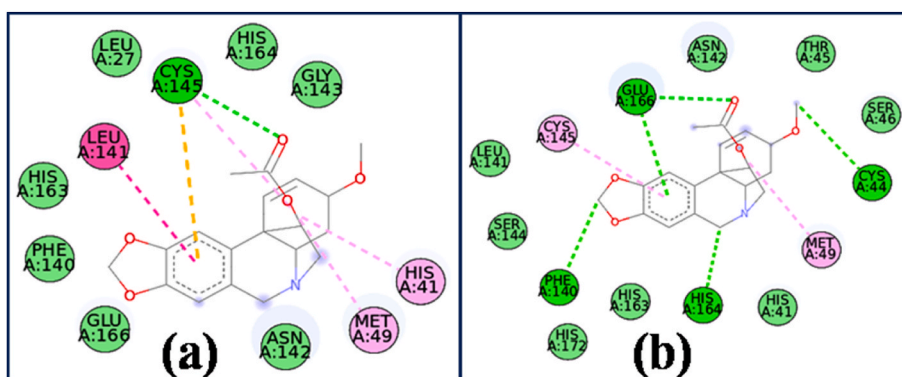


**Fig. 4.** Molecular interaction representation of crinamine acetate with (a) 6LU7 (b) 6Y2E protein. Violet and pink dotted bonds show hydrophobic interaction, green dotted bonds show hydrogen bonds, and electrostatic interaction is shown by deep yellow dotted bond. (For interpretation of the references to color in this figure legend, the reader is referred to the Web version of this article.)
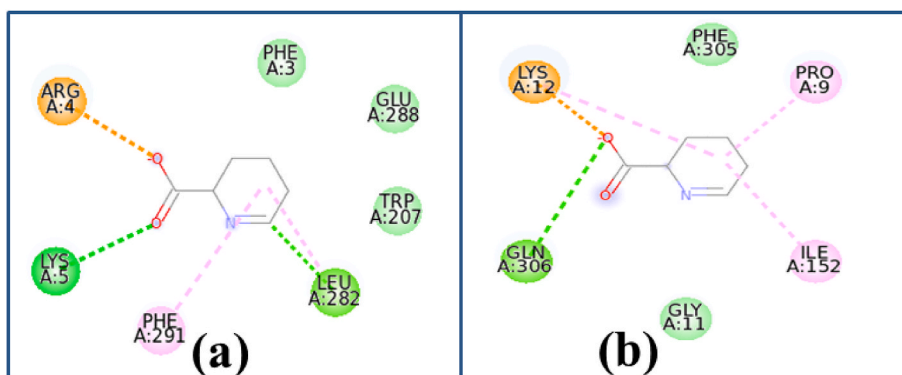


**Fig. 5.** Molecular interaction representation of (S)-1-Piperideine-6-carboxylate with (a) 6LU7 (b) 6Y2E. Violet and pink dotted bonds show hydrophobic interaction, green dotted bonds show hydrogen bonds, and electrostatic interaction is shown by deep yellow dotted bond. (For interpretation of the references to color in this figure legend, the reader is referred to the Web version of this article.)

C–H interaction and -donor hydrogen bonding interaction with bond lengths ranging from 3.08 to 3.90.Å. The amino acid residue MET49 interacted with the ligand through hydrophobic contact with a bond length of 4.31 Å. Fig. 2(a) portrays a graphical diagram of the above relationship. -6.96 kcal/mol was measured as the binding energy of the protease protein 6Y2E with the constituent compound acacetin. The ligand was bound to eight residues (THR26, GLY143, GLU166, HIS164, LEU141, SER144, THR24, and CYS145) by standard hydrogen bonding with bond lengths ranging from 1.96 to 3.32 Å. The HIS41 residue has only one hydrophobic interaction with a bond length of 5.50 Å. In Fig. 2

(b), the linking mode for such an interaction is depicted schematically.

The binding energy performance was estimated -6.93 kcal/mol for protein 6LU7 and indomethacin with bond length of 1.99 and 3.37 Å. ARG188 and MET49 are involved in hydrogen bonding. Hydrophobic interaction was involving MET165 and MET49 residues with bond lengths ranging from 5.50 to 4.70 Å. The ligand was bound to the CYS 145 binding residue by -sulphur bonds with a bond angle of 5.22 Å. Fig. 3 (a) depicts a graphical diagram of the above relationship. The binding energy of 6Y2E with the phytocompound indomethacin was found to be -6.82 kcal/mol. Hydrogen bonding is involved in THR304,
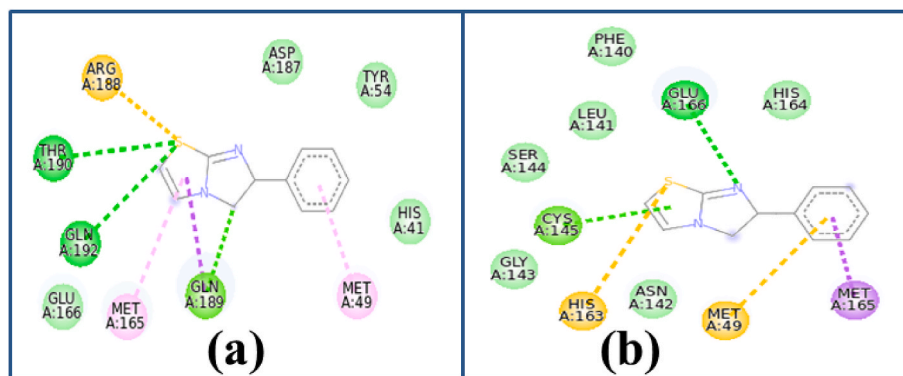
**Fig. 6.** Levamisole's molecular interactions with (a) 6LU7 and (b) 6Y2E. Hydrophobic interaction is represented by violet and pink dotted bonds, hydrogen bonds are represented by green dotted bonds, and electrostatic interaction is represented by a deep yellow dotted bond. (For interpretation of the references to color in this figure legend, the reader is referred to the Web version of this article.)
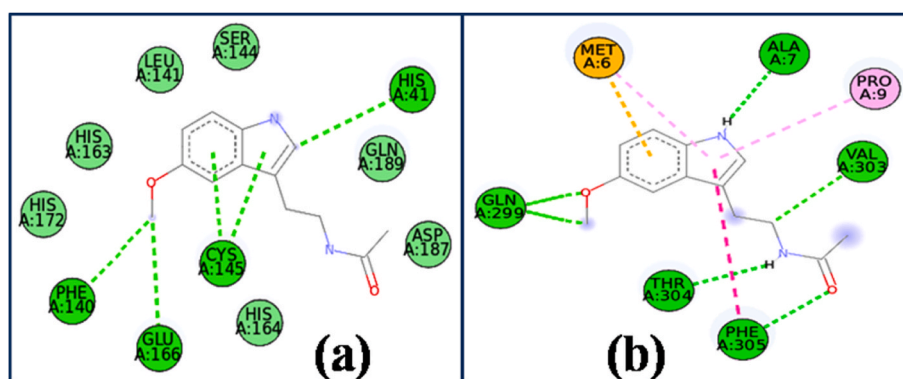


**Fig. 7.** Melatonin's molecular interactions with (a) 6LU7 and (b) 6Y2E. Hydrophobic interaction is represented by violet and pink dotted bonds, hydrogen bonds are represented by green dotted bonds, and electrostatic interaction is represented by a deep yellow dotted bond. (For interpretation of the references to color in this figure legend, the reader is referred to the Web version of this article.)

GLN299, GLY302, and MET6 with bond lengths ranging from 1.80 to 3.27 Å. Hydrophobic interaction involving PHE405, MET6, and PRO9 with bond lengths ranging from 3.73 to 5.43 Å. The linking mode for such an interaction was depicted in Fig. 3 (b).

The binding energy of the protein 6LU7 with the compound crinamine acetate was -7.6 kcal/mol. The N-atom of the ligand was interacted with the CYS145 residue by conventional H-bonding with a bond length 3.05 Å and the residues LEU141, ASN142, MET49, CYS145 and HIS41 contains hydrophobic contacts with the binding sites of the ligand with varying bond lengths from 4.59 to 5.28 Å. The interaction study was depicted in the Fig. 4(a). The binding energy of 6Y2Emainprotease protein with the compoundcrinamine acetate is -7.38 kcal/mol. GLU166, HIS164, PHE140 and CYS44 amino acid residues is connected by H-bonding of bond length 2.69 to 3.92 Å. MET49 and CYS145 residues are involved in hydrophobic interaction with the ligand molecule through alkyl and π -alkyl stacking with a bond length of 4.85 and 4.80 Å. Schematic representation of the binding mode is shown in the Fig. 4 (b).

The protease protein 6LU7binding energy with compound (S)-1-Piperideine-6-carboxylate was measured to be -4.44 kcal/mol. ARG4 residue involved in electrostatic interaction with bond length 2.91 Å. LYS5 and LEU282 involved in hydrogen bonding with bond length 2.79 and 3.28 Å. LEU282 and PHE291 involved in hydrophobic interaction with a bond length of 5.33 and 4.94 Å. Schematic representation of the binding mode is given in the Fig. 5 (a). 6Y2E has a binding energy of -4.51 kcal/mol with the phytocompound (S)-1-Piperideine-6-carboxylate. With a bond length of 2.60 Å, the LYS12 binding residue is involved in electrostatic interaction with the ligands.With a bond length

of 3.59 Å, the GLN306 residue is involved in hydrogen bonding. PRO9, LYS12, and ILE152 residues interact hydrophobically with bond lengths ranging from 3.76 to 4.79 Å. Fig. 5(b) shows a schematic representation of the binding mode.

The binding energy of the protease protein 6LU7 with the compound levamisole was determined to be -5.83 kcal/mol. THR190, GLN192, and GLN189 are all involved in hydrogen bonding with 3.67, 3.78, and 3.47 Å bond lengths. With a bond length ranging from 3.76 to 4.49 Å, GLN189 is also involved in hydrophobic interaction with MET165 and MET49 residue. Fig. 6(a) shows a representation of the binding mode (a). 6Y2E has a binding energy of -5.82 kcal/mol with the same phytocompound. With bond lengths of 2.86 and 3.34 Å, GLU166 and CYS145 residues are involved in hydrogen bonding. With bond lengths of 3.45 and 3.81 Å, MET165 is involved in hydrophobic interactions. Fig. 6 (b) depicts a schematic representation of such a binding mode.

The binding energy of the protease protein 6LU7 with the compound Melatonin was estimated to be -5.62 kcal/mol. Hydrogen bonding occurs between HIS41, PHE140, GLU166, and CYS145 residues, with bond lengths ranging from 3.25 to 3.78 Å. Fig. 7 (a) shows a representation of the binding mode with the same phytocompound, 6Y2E has a binding energy of -5.38 kcal/mol. The residues PHE305, THR304, GLN299, and VAL303 are involved in hydrogen bonding interactions with bond lengths ranging from 2.17 to 3.38 Å. With bond lengths ranging from 4.62 to 5.17, PHE305, PRO9, and MET6 are involved in a hydrophobic relationship. The π-sulphur bond, which has a bond length of 4.02 Å, is also present in MET6. Fig. 7 (b) depicts a schematic depiction of such a binding mode.

The protease protein 6LU7 binding energy with compound Nicotinic
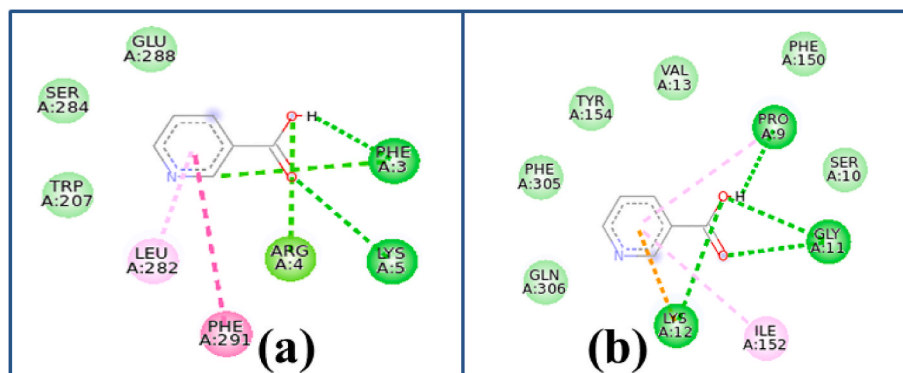
**Fig. 8.** Molecular interaction representation of nicotinic acid with (a) 6LU7 (b) 6Y2E protein. Violet and pink dotted bonds show hydrophobic interaction, green dotted bonds show hydrogen bonds, and electrostatic interaction is shown by deep yellow dotted bond. (For interpretation of the references to color in this figure legend, the reader is referred to the Web version of this article.)
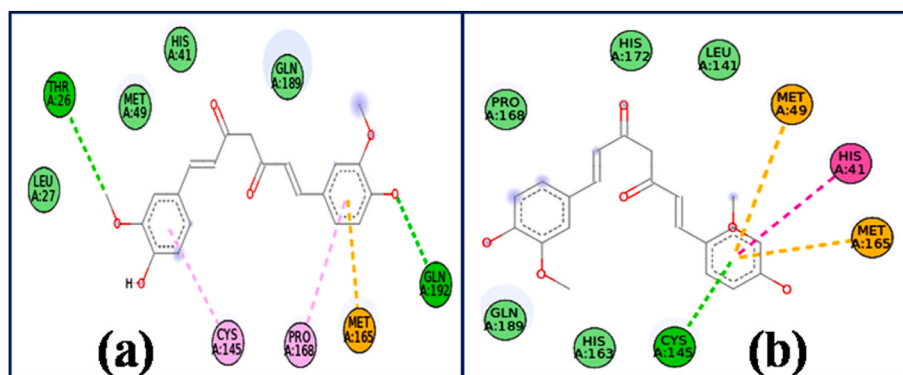


**Fig. 9.** Molecular interaction representation of curcumin with (a) 6LU7 (b) 6Y2E protein. Violet and pink dotted bonds show hydrophobic interaction, green dotted bonds show hydrogen bonds, and electrostatic interaction is shown by deep yellow dotted bond. (For interpretation of the references to color in this figure legend, the reader is referred to the Web version of this article.)
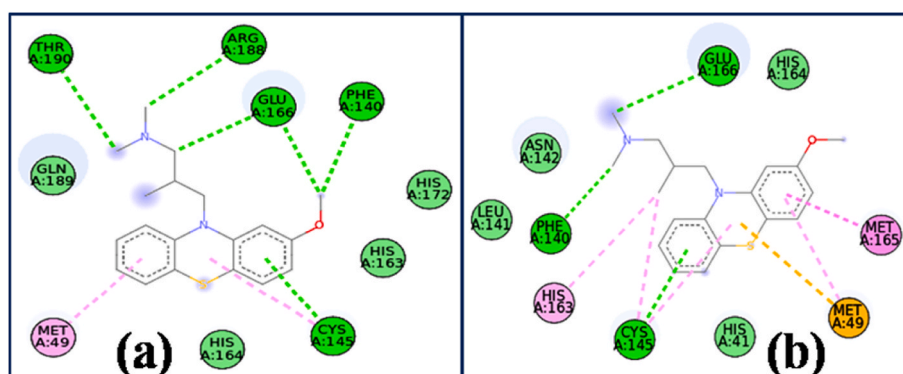


**Fig. 10.** Molecular interaction representation of methotrimeprazine with (a) 6LU7 (b) 6Y2E. Violet and pink dotted bonds show hydrophobic interaction, green dotted bonds show hydrogen bonds, and electrostatic interaction is shown by deep yellow dotted bond. (For interpretation of the references to color in this figure legend, the reader is referred to the Web version of this article.)

acid is measured to be -4.33 kcal/mol. LYS5, PHE3 and ARG4 residues involved in hydrogen bonding with bond length from 1.90 to 3.44 Å. PHE291 and LEU 282 involved in hydrophobic interaction. The bond length for such interaction is 5.13 and 5.61 Å respectively. The binding mode representation is shown in the Fig. 8(a). The binding energy of 6Y2E with the same phytocompound is measured -4.18 Å. GLY11, LYS12 and PRO9 residues concerned in hydrogen bonding. The bond length for such interaction is varied from 1.78 to 2.98 Å. LYS12 is involved in electrostatic interaction with bond length 3.56 Å and PRO9, LYS12 and ILE152 occupied in hydrophobic interaction with bond length varied

from 4 to 5.02 Å. The schematic representation of such binding mode is shown in Fig. 8(b).

The binding energy for the protease protein 6LU7 with the phytocompound Curcumin is -6.78 kcal/mol. GLN192 and THR26 involved in hydrogen bonding with bond length 2.84 and 3.53 Å. Met165 involved in pi-sulphur bonding interaction with bond length 5.11 Å. PRO165 and CYS145 involved in hydrophobic interaction. The bond length for such interaction is 4.93 and 5.01 Å respectively. The binding mode for such interaction is shown in the schematic Fig. 9(a). The protease protein 6Y2E binding energy with compound is -5.67 kcal/mol. CYS145 binding
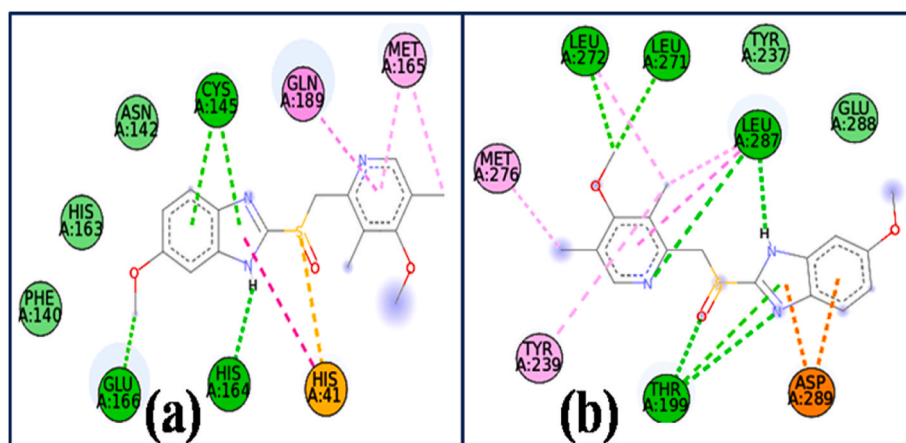
**Fig. 11.** Molecular interaction representation of omeprazole with (a) 6LU7 (b) 6Y2E Violet and pink dotted bonds show hydrophobic interaction, green dotted bonds show hydrogen bonds, and electrostatic interaction is shown by deep yellow dotted bond. (For interpretation of the references to color in this figure legend, the reader is referred to the Web version of this article.)
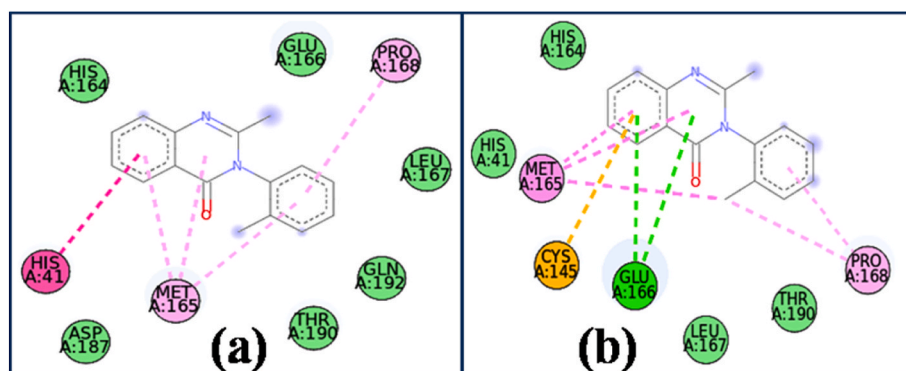


**Fig. 12.** Molecular interaction representation of methaqualone with (a) 6LU7 (b) 6Y2E protein. Violet and pink dotted bonds show hydrophobic interaction, green dotted bonds show hydrogen bonds, and electrostatic interaction is shown by deep yellow dotted bond. (For interpretation of the references to color in this figure legend, the reader is referred to the Web version of this article.)

residue has involved in hydrogen bonding 3.81 Å. HIS41 occupied in hydrophobic interaction with bond length 4.37 Å and MET165 and MET49 occupied in π-sulphur bonding with varying bond length from 5.12 to 7.72 Å. The schematic diagram of the above interaction is shown in Fig. 9(b).

The binding energy of 6LU7 with compound Methotrimeprazine is measured to be -6.96 kcal/mol. GLU166, THR190, ARG188, PHE140 and CYS145 occupied in hydrogen bonding with bond length varying from 3.22 to 3.83 Å. CYS145 and MET49 involved in hydrophobic interaction with bond length 4.87 and 5.18 Å. The schematic diagram of the above interaction is shown in Fig. 10(a). The binding energy measured for the protease protein 6Y2E with the phytocompound methotrimeprazine is -6.76 kcal/mol. PHE140, GLU166 and CYS145 associated in hydrogen bonding. The bond length for such interaction is varied from 3.19 to 3.67 Å. MET165, CYS145, MET49 and HIS163 residues associated in hydrophobic interaction with bond length from 3.90 to 5.12 Å. MET49 is also involved in π -sulphur interaction with bond length 5.17 Å.The binding mode for such interaction is shown in the schematic Fig. 10(b).

The binding energy of 6LU7 with Omeprazole is -7.12 kcal/mol. HIS164, GLU166 and CYS145 residues are interacted via hydrogen bond with the ligand with bond length from 1.87 to 3.78 Å. GLN189 and MET165 involved in hydrophobic interaction with bond length from 3.35 to 4.25 Å and HIS 41 involved in pi-sulphur bonding interaction with bond length 5.14 Å.The binding mode for such interaction is shown in the schematic Fig. 11(a). Binding energy of 6Y2E with the same

phytocompound -6.26 kcal/mol. THR199, LEU287, LEU271 and LEU272 associated in hydrogen bonding with bond length varies from 1.83 to 4.82 Å. ASP289 associated in electrostatic interaction with bond length 3.26 and 4.82 Å. The binding residues involved in hydrophobic interactions such as LEU287, MET276, LEU272 and TYR239. The bond lengths are varied from 3.69 to 5.25 Å. The binding mode for such interaction is shown in the schematic Fig. 11(b).

The protease protein 6LU7 binding energy with compound methaqualone is -6.93 kcal/mol. HIS41, MET165 and PRO168 residues are involved in hydrophobic interaction with bond length varies from 4.18 to 5.08 Å. No hydrogen bonding and electrostatic interactions are found here. The schematic diagram of the above interaction is shown in Fig. 12 (a). Binding energy for the protease protein 6Y2E with the phytocompound methaqualone is -6.59 kcal/mol. GLU166 associated in hydrogen bonding with bond length 3.79 and 3.99 Å. MET165 and PRO168 associated in hydrophobic interaction with a varying of bond length of 3.96 to 5.13 Å. CYS145 is associated in π -sulphur bonding with bond length 5.47 Å. The binding mode for such interaction is shown in the schematic Fig. 12 (b).The detailed binding properties of the screened phytochemicals with main protease 6LU7 and 6Y2Eare mentioned in Table 4 and Table 5 respectively.

In the present study we have observed the interactions of our reported phytochemicals with the mutated spike RBD of SARS-CoV-2. The mutant and the phytochemical thebaine interaction results a binding energy of -7.24 kcal/mol. The residues TYR365 and ALA363 established strong hydrogen bonding with a bond length of 2.16 to 2.3 Å (Fig. S1).

**Table 4**
Binding energies, residues during interaction of phytochemicals with 6LU7.

| Phytochemicals | Binding energy (kcal/mol) | Binding residues | Bond length (Å) |
|---|---|---|---|
| Thebaine | - 6.93 | GLU166:N - LIG1:O | 2.87 |
| | | LIG1:C – HIS41:NE2 | 3.55 |
| | | LIG1:C – GLN189:OE1 | 3.27 |
| | | LIG1:C - PHE140:O | 3.11 |
| | | LIG1:C - GLU166:OE2 | 3.29 |
| | | CYS145:SG - LIG1 | 3.79 |
| | | CYS145 - LIG1 | 5.36 |
| | | CYS145 - LIG1 | 4.37 |
| | | HIS41 - LIG1 | 5.49 |
| Acacetin | −7.77 | LIG1:H - LEU141:O | 1.67 |
| | | HIS172:CD2 - LIG1:O | 3.76 |
| | | LIG1:C - MET49:O | 3.49 |
| | | LIG1:C - TYR54:OH | 3.08 |
| | | CYS145:SG - LIG1 | 3.32 |
| | | CYS145:SG - LIG1 | 3.90 |
| | | LIG1 - MET49 | 4.61 |
| Indomethacin | −6.39 | LIG1:H - ARG188:O | 1.99 |
| | | LIG1:C - MET49:O | 3.37 |
| | | LIG1:C - MET165 | 4.57 |
| | | LIG1 - MET165 | 4.50 |
| | | LIG1 - MET49 | 4.70 |
| | | LIG1 - CYS145 | 5.22 |
| Crinamine acetate | −7.6 | CYS145:N - LIG1:O | 3.05 |
| | | LEU141:C,O;ASN142:N-LIG1MET49 - LIG1 | 4.59 |
| | | | 5.27 |
| | | CYS145 - LIG1 | 5.28 |
| | | HIS41 - LIG1 | 4.70 |
| (S)-1-Piperideine-6-carboxylate | - 4.44 | ARG4:NH1 – UNK0:O | 2.91 |
| | | LYS5:N -:UNK0:O | 2.79 |
| | | UNK0:C - LEU282:O | 3.28 |
| | | LEU282 -:UNK0 | 5.33 |
| | | PHE291 -:UNK0 | 4.94 |
| Levamisole | −5.83 | THR190:N – UNK0:S | 3.67 |
| | | GLN192:NE2 -UNK0:S | 3.78 |
| | | UNK0:C -GLN189:OE1 | 3.47 |
| | | GLN189:CA - UNK0 | 2.96 |
| | | UNK0 - MET165 | 3.76 |
| | | UNK0 - MET49 | 4.49 |
| Melatonin | −5.62 | LIG1:C – HIS41:NE2 | 3.78 |
| | | LIG1:C - PHE140:O | 3.25 |
| | | LIG1:C - GLU166:OE2 | 3.32 |
| | | CYS145:SG - LIG1 | 3.27 |
| | | CYS145:SG - LIG1 | 3.62 |
| Nicotinic acid | - 4.33 | LYS5:N – UNK0:O | 2.87 |
| | | UNK0:H - PHE3:O | 1.90 |
| | | ARG4:CD - UNK0:O | 3.06 |
| | | UNK0:C - PHE3:O | 3.44 |
| | | PHE291 - UNK0 | 5.62 |
| | | UNK0 - LEU282 | 5.13 |
| Curcumin | −6.78 | GLN192:N - LIG1:O | 2.84 |
| | | LIG1:C - THR26:O | 3.53 |
| | | LIG1 - MET165 | 5.11 |
| | | LIG1 - PRO168 | 5.01 |
| | | LIG1 - CYS145 | 4.93 |
| Methotrimeprazine | −6.96 | LIG1:C - GLU166:O | 3.22 |
| | | LIG1:C - THR190:O | 3.79 |
| | | LIG1:C - ARG188:O | 3.55 |
| | | LIG1:C - PHE140:O | 3.26 |
| | | LIG1:C -GLU166:OE2 | 3.74 |
| | | CYS145:SG - LIG1 | 3.83 |
| | | LIG1 - CYS145 | 5.18 |
| | | LIG1 - MET49 | 4.87 |
| Omeprazole | −7.12 | LIG1:H – HIS164:O | 1.87 |
| | | LIG1:C - GLU166:OE2 | 2.37 |
| | | CYS145:SG - LIG1 | 3.39 |
| | | CYS145:SG - LIG1 | 3.78 |
| | | GLN189:CG - LIG1 | 3.35 |
| | | HIS41 -:LIG1 | 5.14 |
| | | LIG1:C - MET165 | 3.70 |
| | | LIG1 - MET165 | 4.34 |
| Methaqualone | −6.93 | HIS41 - LIG1 | 4.72 |
| | | LIG1 - MET165 | 4.18 |
| | | LIG1 - MET165 | 4.81 |
| | | LIG1 - MET165 | 5.03 |
| | | LIG1 - PRO168 | 5.08 |

**Table 5**
Binding energies, residues during interaction of phytochemicals with 6Y2E.

| Chemical compounds | Binding energy (kcal/mol) | Binding residues | Bond length (Å) |
|---|---|---|---|
| Thebaine | −7.28 | GLU166:N - LIG1:O | 2.97 |
| | | LIG1:C - SER144:OG | 2.84 |
| | | GLU166:OE1 - LIG1 | 4.40 |
| | | CYS145 - LIG1 | 4.48 |
| | | CYS145 - LIG1 | 4.42 |
| | | MET165 - LIG1 | 5.40 |
| | | HIS41 - LIG1 | 4.67 |
| Acacetin | −6.96 | THR26:N - LIG1:O | 3.02 |
| | | GLY143:N - LIG1:O | 3.14 |
| | | GLU166:N - LIG1:O | 2.77 |
| | | LIG1:H – HIS164:O | 2.99 |
| | | LIG1:H - LEU141:O | 2.03 |
| | | LIG1:H - SER144:OG | 1.96 |
| | | LIG1:C - THR24:O | 3.13 |
| | | CYS145:SG - LIG1 | 3.32 |
| | | CYS145:SG - LIG1 | 3.22 |
| | | HIS41 - LIG1 | 5.50 |
| Indomethacin | - 6.82 | THR304:OG1 - LIG1:O | 2.74 |
| | | LIG1:H - GLN299:O | 1.80 |
| | | GLY302:CA - LIG1:O | 3.27 |
| | | LIG1:C - MET6:O | 2.86 |
| | | PHE305 - LIG1 | 4.77 |
| | | LIG1:Cl - PRO9 | 3.73 |
| | | LIG1 - MET6 | 4.88 |
| | | LIG1 - PRO9 | 5.43 |
| | | LIG1 - PRO9 | 4.30 |
| Crinamine acetate | −7.38 | GLU166:N - LIG1:O | 2.77 |
| | | LIG1:C – HIS164:O | 2.69 |
| | | LIG1:C - PHE140:O | 3.32 |
| | | LIG1:C – CYS44:O | 3.61 |
| | | GLU166:N - LIG1 | 3.92 |
| | | MET49 - LIG1 | 4.85 |
| | | LIG1 - CYS145 | 4.80 |
| (S)-1-Piperideine-6-carboxylate | - 4.51 | LYS12:N – UNK0:O | 2.60 |
| | | GLN306:C – UNK0:O | 3.59 |
| | | PRO9 - UNK0 | 3.76 |
| | | LYS12 - UNK0 | 4.65 |
| | | ILE152 - UNK0 | 4.79 |
| Levamisole | −5.82 | GLU166:N – UNK0:N | 2.86 |
| | | CYS145:SG - UNK0 | 3.34 |
| | | MET165:CE - UNK0 | 3.81 |
| | | MET165:CE:B – UNK0 | 3.45 |
| Melatonin | −5.38 | PHE305:N - LIG1:O | 2.95 |
| | | LIG1:H - ALA7:O | 2.17 |
| | | LIG1:H - | 2.31 |
| | | | 2.96 |

**Table 5** (*continued*)

| Chemical compounds | Binding energy (kcal/mol) | Binding residues | Bond length (Å) |
|---|---|---|---|
| | | THR304:OG1 | 3.62 |
| | | GLN299:CA - LIG1:O | 3.38 |
| | | LIG1:C - VAL303:O | 5.17 |
| | | LIG1:C - GLN299:O | 4.62 |
| | | LIG1 - PHE305 | 4.90 |
| | | LIG1 - MET6 | 4.02 |
| | | LIG1 - PRO9 | |
| | | LIG1 - MET6 | |
| Nicotinic acid | - 4.18 | GLY11:N – UNK0:O | 2.95 |
| | | GLY11:N – UNK0:O | 2.79 |
| | | LYS12:N – UNK0:O | 2.68 |
| | | UNK0:H - PRO9:O | 1.78 |
| | | LYS12:NZ - UNK0 | 3.56 |
| | | UNK0 - PRO9 | 4.88 |
| | | UNK0 - LYS12 | 4.00 |
| | | UNK0 - ILE152 | 5.02 |
| Curcumin | −5.67 | CYS145:SG - LIG1 | 3.81 |
| | | HIS41 - LIG1 | 4.37 |
| | | LIG1 – MET165 | 5.12 |
| | | LIG1 - MET49 | 7.72 |
| Methotrimeprazine | - 6.76 | LIG1:C - PHE140:O | 3.19 |
| | | LIG1:C - GLU166:OE1 | 3.49 |
| | | CYS145:SG - LIG1 | 3.67 |
| | | MET165:CE:B - LIG1 | 3.90 |
| | | LIG1:C – CYS145 | 4.47 |
| | | HIS163 - LIG1:C | 4.66 |
| | | LIG1 - MET49 | 5.17 |
| | | LIG1 - CYS145 | 5.12 |
| | | LIG1 - MET49 | 4.99 |
| | | LIG1 - MET165 | 4.51 |
| Omeprazole | - 6.26 | THR199:OG1 - LIG1:O | 2.75 |
| | | THR199:OG1 - LIG1:N | 3.35 |
| | | LEU287:N - LIG1:N | 2.84 |
| | | LIG1:H - LEU287:O | 1.83 |
| | | LIG1:C - LEU271:O | 3.03 |
| | | LIG1:C - LEU272:O | 3.29 |
| | | ASP289:OD1 - LIG1 | 3.26 |
| | | ASP289:OD2 - LIG1 | 4.82 |
| | | THR199:OG1 - LIG1 | 3.99 |
| | | LEU287:CD1 - LIG1 | 3.69 |
| | | LIG1:C - MET276 | 5.06 |
| | | LIG1:C - LEU272 | 4.56 |
| | | LIG1:C - LEU287 | 5.25 |
| | | TYR239 - LIG1:C | 5.10 |
| Methaqualone | - 6.59 | GLU166:N - LIG1 | 3.79 |
| | | GLU166:N - LIG1 | 3.99 |
| | | MET165:CA - LIG1 | 3.86 |
| | | | 3.96 |
| | | | 4.91 |
| | | | 4.61 |

**Table 5** (*continued*)

| Chemical compounds | Binding energy (kcal/mol) | Binding residues | Bond length (Å) |
|---|---|---|---|
| | | MET165:C- LIG1 | 5.13 |
| | | LIG1:C - MET165 | 5.47 |
| | | LIG1:C - PRO168 | 4.42 |
| | | LIG1 - MET165 | |
| | | LIG1 - CYS145 | |
| | | LIG1 - PRO168 | |

From the figure it was seen that some residues are involved in hydrophobic interaction. These are PHE338, TYR365, ALA363, VAL367, LEU368, LEU335, and PHE338 with a varying bond length of 3.62 to 5.48 Å. The residue ASP364 shows electrostatic interaction with a bond length of 3.62 Å.The interaction of phytocompound acacetin and the mutant results binding energy -7.75 kcal/mol. In addition, we observed that CYS336, TYR365, ASP364 and ALA363 established strong hydrogen bond with bond length varying from 1.85 to 2.7 Å. The residues VAL367, LEU368, CYS336 and ALA363 exhibit hydrophobic interaction with the mutant protein with the bond length of 4.31 to 5.39 Å (Fig. S2).The binding energy was estimated -6.56 kcal/mol for the indomethacin and the mutant spike RBD interaction. It was observed from the Fig. S3, the residues LYS444, TYR449, ARG452, ASN448 and ASN450 exhibit strong hydrogen bonding with bond length from 1.72 to 3.01 Å. TYR449 exhibit hydrophobic interaction with bond length 4.72 and 5.26 Å. Binding energy was estimated to be -6.71 kcal/mol for the crinamineacetate and mutant spike RBD interaction. GLY339 residue exhibits hydrogen bonding interaction with the bond length of 2.43 Å. In addition to this, the residues PHE342, PHE338, GLY339, VAL367 and LEU368 of the ACE2 exhibit hydrophobic interaction of varying bond length 4.33 to 5.97 Å. Figs. S4 and S5 represents the binding interaction of the mutant protein with the (S)-1-Piperideine-6-carboxylate. Binding energy results -4.91 kcal/mol for such interaction. ARG403 shows a little electrostatic interaction with bond length 4.56 Å, ARG403, PHE497 and TYR505 exhibit hydrophobic interaction with bond length 4.64, 5.12 and 5.17 Å respectively. ARG403 and GLY496 exhibit strong hydrogen bonding with the phytocompound with bond length 1.85 to 2.21 Å. Binding energy performance was estimated -5.83 kcal/mol for the phyotocompound levamisole and the mutant protein. The interaction is shown in Fig. S6. GLN474, GLU471 and ILE472 residues associated with hydrogen bonding with bond length 1.93, 3.11 and 3.5 Å respectively. In addition to this, LYS458, TYR473 and ARG457 involved in electrostatic as and hydrophobic interaction with bond length from 4.63 to 5.02 Å. The interaction of phytocompound melatonin and the mutant results binding energy -5.38 kcal/mol. In addition, we observed that CYS336, TYR365, and GLY339 established strong hydrogen bond with bond length varying from 2.11 to 2.37 Å. The residues PHE342, LEU335, CYS336 and ALA363 exhibit hydrophobic interaction with the mutant protein with the bond length of 3.87 to 5.47 Å (Fig. S7). It is observed from the interaction of nicotinic acid and the mutant protein the binding energy performance is lowest (-4.84 kcal/mol) among all other phytocompounds. Nicotinic acid is associated with hydrogen bonding interaction with ASN450 and GLY447 with bond 1.94 and 2.13 Å respectively. The interaction is shown in the Fig. S8.Curcumin interaction with mutant RBD results binding energy -6.19 kcal/mol (Fig. S9). It is observed that curcumin is associated with hydrogen bond interaction with ASP364, TYR365, ALA363 and VAL367 with bond length 2.11 to 3.4 Å. Other than the hydrogen bond interaction, the curcumin is stabilized by hydrophobic interaction with the residues PHE342, LEU335 and VAL367. The bond length was varying from 4.74 to 5.42 Å for this interaction. The binding energy performance estimated -6.26 kcal/mol for Methotrimeprazine and mutant RBD (Fig. S10). The residues ASP364, VAL362 and CYS336 associated with hydrogen bond interaction with methotrimeprazine. In addition to this, PHE338, VAL376,

**Table 6**
Binding energies, residues during interaction of phytochemicals with mutant of receptor binding domain of spike protein.

| Chemical compounds | Binding energy (kcal/mol) | Binding Residues | Bond length (Å) |
|---|---|---|---|
| Thebaine | −7.24 | TYR365 | 2.16 |
| | | ALA363 | 2.05 |
| | | ALA363 | 2.30 |
| | | ASP364 | 3.62 |
| | | PHE338 | 3.60 |
| | | TYR365 | 3.92 |
| | | ALA363 | 4.63 |
| | | VAL367 | 5.08 |
| | | VAL367 | 4.67 |
| | | VAL367 | 4.90 |
| | | LEU368 | 5.13 |
| | | LEU335 | 5.48 |
| | | PHE338 | 5.35 |
| | | LEU335 | 4.96 |
| Acacetin | −7.75 | CYS336 | 2.75 |
| | | TYR365 | 2.65 |
| | | ASP364 | 1.85 |
| | | CYS336 | 1.70 |
| | | ALA363 | 2.70 |
| | | TYR365 | 2.55 |
| | | VAL367 | 4.31 |
| | | LEU368 | 5.17 |
| | | CYS336 | 5.31 |
| | | ALA363 | 4.96 |
| | | VAL367 | 5.39 |
| Indomethacin | −6.56 | LYS444 | 1.90 |
| | | TYR449 | 1.72 |
| | | ARG452 | 2.21 |
| | | ARG452 | 1.89 |
| | | ASN448 | 2.85 |
| | | ASN450 | 3.01 |
| | | TYR449 | 2.89 |
| | | TYR449 | 5.26 |
| | | TYR449 | 4.72 |
| Crinamine acetate | −6.71 | GLY339 | 2.43 |
| | | PHE342 | 5.97 |
| | | PHE338 | 4.33 |
| | | GLY339 | 4.33 |
| | | VAL367 | 4.96 |
| | | VAL367 | 4.45 |
| | | LEU368 | 5.21 |
| (S)-1-Piperideine-6-carboxylate | −4.91 | ARG403 | 4.56 |
| | | ARG403 | 2.21 |
| | | ARG403 | 1.85 |
| | | GLY496 | 2.05 |
| | | ARG403 | 5.12 |
| | | PHE497 | 5.17 |
| | | TYR505 | 4.64 |
| Levamisole | −5.83 | GLN474 | 1.93 |
| | | GLU471 | 3.11 |
| | | ILE472 | 3.50 |
| | | LYS458 | 4.91 |
| | | TYR473 | 5.02 |
| | | LYS458 | 4.63 |
| | | ARG457 | 4.64 |
| Melatonin | −5.38 | TYR365 | 2.11 |
| | | CYS336 | 2.21 |
| | | GLY339 | 2.37 |
| | | PHE342 | 3.87 |
| | | LEU335 | 5.47 |
| | | CYS336 | 5.15 |
| | | ALA363 | 4.36 |
| Nicotinic acid | −4.84 | ASN450 | 2.13 |
| | | GLY447 | 1.94 |
| Curcumin | −6.19 | ASP364 | 2.13 |
| | | TYR365 | 2.11 |
| | | ALA363 | 2.49 |
| | | TYR365 | 2.41 |
| | | VAL367 | 3.40 |
| | | PHE342 | 4.74 |
| | | LEU335 | 5.42 |

**Table 6** (*continued*)

| Chemical compounds | Binding energy (kcal/mol) | Binding Residues | Bond length (Å) |
|---|---|---|---|
| | | VAL367 | 5.01 |
| | | LEU368 | 5.18 |
| Methotrimeprazine | −6.26 | ASP364 | 2.93 |
| | | VAL362 | 2.92 |
| | | CYS336 | 3.09 |
| | | ASP364 | 4.96 |
| | | ASP364 | 4.27 |
| | | PHE338 | 5.79 |
| | | PHE338 | 4.28 |
| | | VAL367 | 5.19 |
| | | VAL367 | 5.18 |
| | | ALA363 | 4.30 |
| | | LEU368 | 4.75 |
| Omeprazole | −6.3 | ARG454 | 2.47 |
| | | GLU471 | 2.29 |
| | | SER459 | 3.54 |
| | | GLN474 | 3.11 |
| | | GLU471 | 4.78 |
| | | GLN474 | 2.96 |
| | | TYR473 | 5.87 |
| | | ARG457 | 3.28 |
| | | LYS458 | 4.69 |
| Methaqualone | −6.34 | PHE338 | 5.17 |
| | | PHE338 | 4.98 |
| | | GLY339 | 4.98 |
| | | VAL367 | 3.78 |
| | | VAL367 | 3.98 |
| | | LEU368 | 4.24 |
| | | VAL367 | 3.90 |
| | | VAL367 | 5.02 |
| | | CYS336 | 5.07 |
| | | ALA363 | 4.42 |
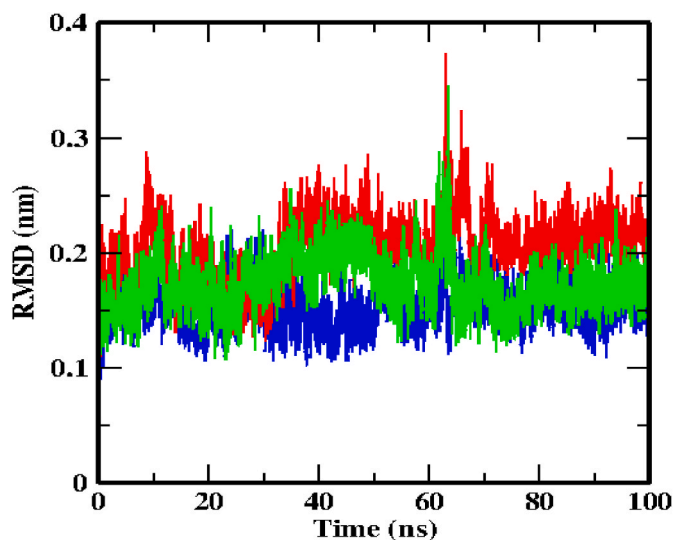


**Fig. 13.** RMSD plot of backbone atoms for 6LU7-acacetin (red color), 6Y2E-acacetin system (bluecolor) and spikeRBD-acacetin (green color). (For interpretation of the references to color in this figure legend, the reader is referred to the Web version of this article.)

ALA363 and LEU368 residues is stabilized by hydrophobic bonds with bond length 4.3 to 5.79 Å. ASP364 is associated in electrostatic interaction with methotrimeprazine.The phytocompound Omeprazole and the mutant spike RBD interaction results binding affinity -6.3 kcal/mol (Fig. S11). ARG454, GLU471, SER459 and GLN474 connected with hydrogen bonding interaction with omeprazole with bond length 2.29 to 3.54 Å. The residue GLU471 is also associated with electrostatic interaction. In addition to this TYR473 and ARG457, LYS458 engaged with pi-sulphur and hydrophobic interaction with bond length 5.87, 3.28 and
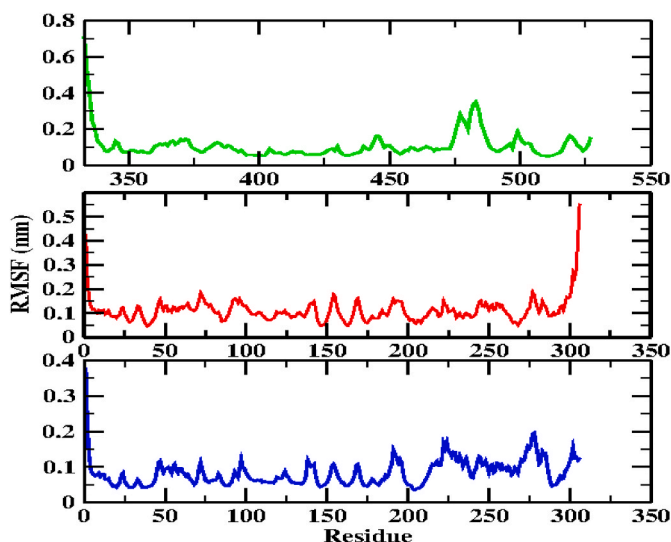
**Fig. 14.** RMSF plot of backbone atoms for 6LU7- acacetin (red color), 6Y2E-acacetin system (blue color) and spike RBD-acacetin (green color). (For interpretation of the references to color in this figure legend, the reader is referred to the Web version of this article.)



**Fig. 16.** Radius of gyration plot of backbone atoms for 6LU7- acacetin (red color), 6Y2E-acacetin system (blue color) and spike RBD-acacetin (green color). (For interpretation of the references to color in this figure legend, the reader is referred to the Web version of this article.)
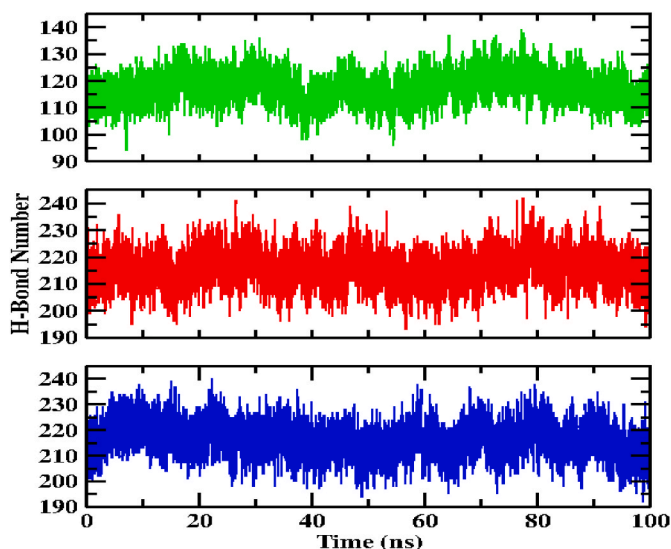


**Fig. 15.** Number of hydrogen bonds present in 6LU7- acacetin (red color), 6Y2E-acacetin system (blue color) and spike RBD-acacetin (green color). (For interpretation of the references to color in this figure legend, the reader is referred to the Web version of this article.)
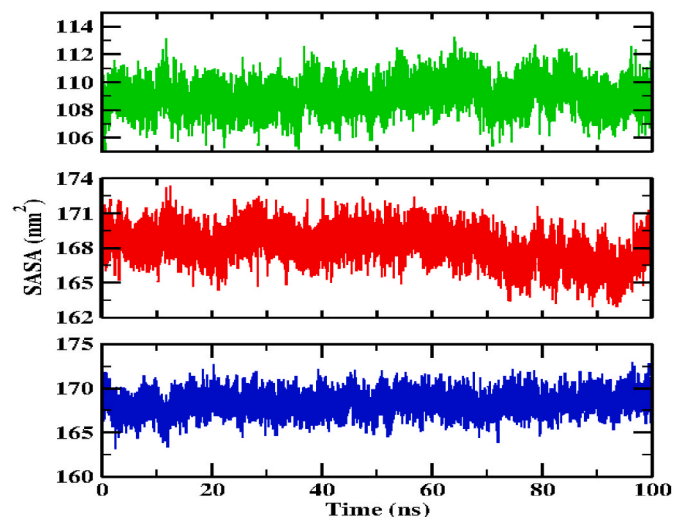


**Fig. 17.** SASA plot of backbone atoms for 6LU7- acacetin (red color), 6Y2E-acacetin system (blue color) and spike RBD-acacetin (green color). (For interpretation of the references to color in this figure legend, the reader is referred to the Web version of this article.)

4.69 Å respectively.The binding energy performance estimated -6.34 kcal/mol for methaqualone and mutant spike RBD (Fig. S12). No hydrogen bond is found in this interaction. All the residues PHE338, GLY339, VAL367, LEU368, CYS336 and ALA363 are stabilized by hydrophobic bonds with bond length varying from 3.78 to 5.17 Å.Binding energies, residues during interaction of phytochemicals with mutant of L4502R E484Q receptor binding domain of Spike protein given in the Table 6.

### 3.3. Molecular dynamics simulation

Molecular dynamics (MD) simulations [68,69] were used to investigate the dynamic properties of the 6LU7-acacetin, 6Y2E-acacetin and spike RBD-acacetin systems. The root mean square deviation (RMSD) of the entire backbone atoms for the above systems was investigated using

**Table 7**

Mean values with standard deviation of RMSD, SASA, Rg, H-bond number of simulation systems.

| Simulation systems | RMSD (nm) | Rg (nm) | SASA(nm$^2$) | H-bond number |
|---|---|---|---|---|
| 6Y2E- acacetin | 0.15 ± 0.02 | 2.18 ± 0.01 | 168.33 ± 1.23 | 216.49 ± 6.4 |
| 6LU7- acacetin | 0.21 ± 0.02 | 2.21 ± 0.02 | 168.19 ± 1.50 | 215.77 ± 6.4 |
| SpikeRBD - acacetin | 0.17 ± 0.02 | 1.86 ± 0.01 | 109.03 ± 1.06 | 117.28 ± 5.50 |
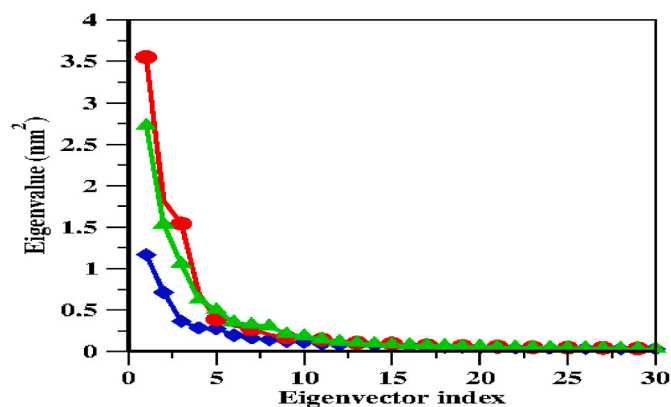
**Fig. 18.** The eigen values plotted alongside the eigenvector index of 6LU7-acacetin (red color), 6Y2E-acacetin system (blue color) and spike RBD-acacetin (green color). (For interpretation of the references to color in this figure legend, the reader is referred to the Web version of this article.)

the gmx rms module. Fig. 13 depicts the RMSD plot. For all the 6LU7-acacetin, 6Y2E-acacetin and Spike RBD-acacetin systems, fluctuation was continued up to 35ns from the RMSD graph during the equilibration time. After 40 ns, the fluctuation pattern of the 6LU7-acacetin system steadily increases, whereas spike RBD-acacetin system increases its stability after 60ns. The RMSD value unexpectedly rises to 0.36 nm at 65 ns.The RMSD value then decreased until it reached a steady state value of 0.22 nm up to 100 ns. RMSD values for the 6Y2E-acacetin system decrease over time as compared to the 6LU7-acacetin system during a 100ns simulation cycle. The average RMSD for the 6Y2E-acacetin system, 6LU7- acacetin system and Spike RBD-acacetin systems were 0.15, 0.21 and 0.17 nm respectively. System stability was characterised by low fluctuations and minimal RMSD values. The RMSD fluctuation analysis indicates that the MD trajectories for the entire studied protein-ligand complex are generally stable and within acceptable ranges during the 100 ns simulation period.

The average movement of the position of an atom at a certain temperature and pressure was measured using Root Mean Square Fluctuation (RMSF). RMSF evaluates regions of structures that fluctuate in relation to the overall structure or identifies a protein's flexible region. During the 100 ns trajectory period, RMSF in constituent residues for 6LU7-acacetin, 6Y2E-acacetin and double mutant of spike RBD-acacetin system was shown in Fig. 14. The fluctuations were observed in the LEU50, ASN72, PRO96, TYR 154, GLY170, ALA 193, ARG 222, and MET 274 residues for both the 6LU7-acacetin and 6Y2E-acacetin systems. In

the spike RBD-acacetin system, fluctuation residues GLY446, SER477, GLY482, THR500, and LEU518 were identified. Higher RMSF values in double mutant of spike RBD-acacetin complex imply more flexibility throughout the MD simulation, whereas a lower RMSF value indicates the system's more stability of 6Y2E-acacetin simulated system.

Generally the formation of hydrogen bonds between a ligand and protein is needed for the ligand-protein complex. The gmx hbond module was used to calculate the average hydrogen bond numbers for 6LU7-acacetin, 6Y2E-acacetin and spike RBD-acacetin systems which was shown in the Fig. 15.It was observed that, 215.77, 216.49 and 117.28 average hydrogen bond numbers for 6LU7-acacetin, 6Y2E-acacetin and spike RBD-acacetin systems respectively. We can say that, acacetin was bound with both 6LU7 and 6Y2E proteins more effectively and tightly as compared to spike RBD protein. The observed higher average hydrogen number of 6Y2E proteins with acacetin which attributed to lower RMSF value.

The radius of gyration (Rg) value determines the compactness of ligand-protein complex. Higher the value of Rg, lower the compactness of the system. The radius of gyration (Rg) of 6LU7-acacetin, 6Y2E-acacetin and Spike RBD-acacetin systems has been observed in Fig. 16. The gmx gyrate code was used to evaluate the Rg properties. The initial computed Rg for the 6LU7- acacetin system is 2.2 nm, and the maximum Rg of 2.28 nm was observed at 5 ns. The fluctuation gradually decreases until it reaches 55 ns.It then increases and preserves the balance until 70ns, when Rg was 2.27 nm. After that, the fluctuation style was gradually reduced until the end of the trajectory, when the Rg value of 2.1 nm was discovered at 100ns. The Rg value for the 6LU7- acacetin system was 2.21 nm on average. Similar fluctuating patterns was also observed in case of Spike RBD-acacetin system where the Rg value was 1.9 nm at 94 ns and the average Rg value 1.86 nm. Whereas, in case of 6Y2E-acacetin system, a steady value of (Rg2.18 nm) was observed throughout the 100ns simulation time leads to more stably bind of 6Y2E with acacetin.

The interaction between complexes and solvents is measured by the solvent accessible surface area (SASA). SASA was computed for ligand-protein complexes to anticipate the extent of conformational changes as well as to calculate the extent of expansion of the protein volume that occurred during the interaction. Fig. 17 depict the time-dependent SASA modifications of 6LU7- acacetin, 6Y2E-acacetin and spike RBD-acacetin systems. The SASA value for the 6LU7- acacetin system varies between 167 and 169 nm$^2$ and the average SASA value for 6Y2E-acacetin and spike RBD-acacetin systems were 168.33 and 109.03 nm$^2$. Here we observed a significant higher value of SASA in case of 6Y2E-acacetin (168.33 nm$^2$) which leads to the 6Y2E protein is more expandable to bind with acacetin in comparison with 6LU7- acacetin and spike RBD-
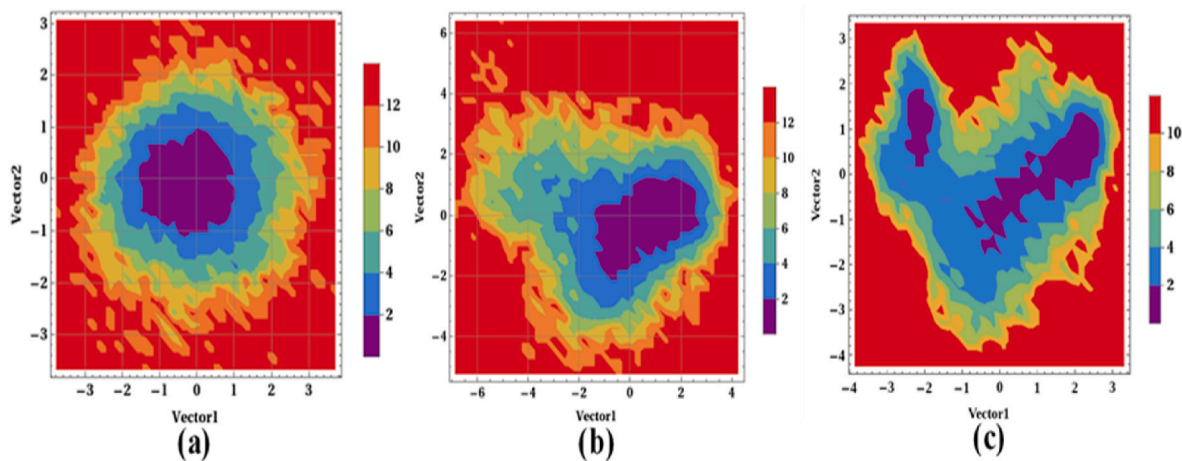


**Fig. 19.** The 2D representation of free energy landscape obtained for PC1 and PC2. (a) represents the 6LU7-acacetin (b) represents 6Y2E-acacetin and (c) represents spike RBD-acacetin system.
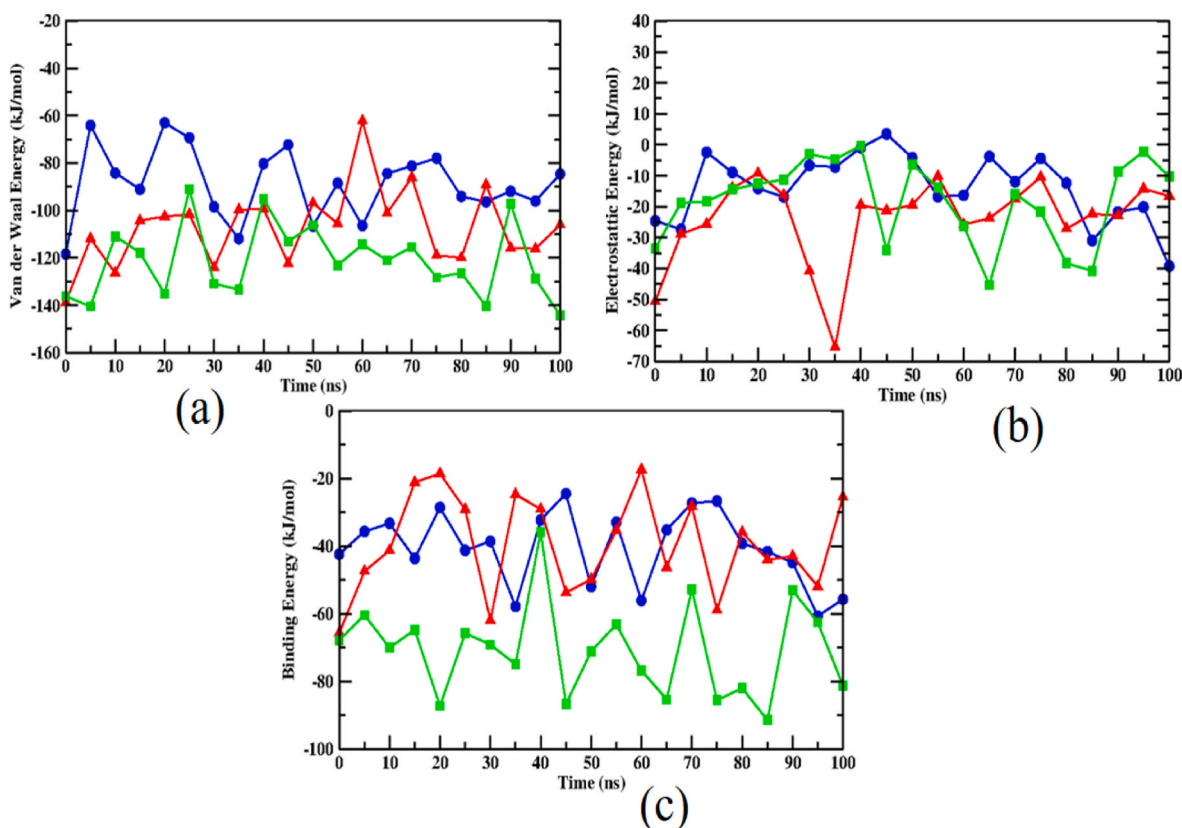
**Fig. 20.** MM-PBSA calculation of (a) Van der Waals energy (b) Electrostatic and (c) Binding energy for 6LU7-acacetin system (red color) 6Y2E-acacetin (blue color) and spike RBD-acacetin (green color). (For interpretation of the references to color in this figure legend, the reader is referred to the Web version of this article.)

**Table 8**
Different average energies obtained from MM-PBSA method of 6LU7, 6Y2E system and Spike RBD.

| Different energy(kJ/ mol) | 6Y2E system | 6LU7 system | Mutant SpikeRBD system |
|---|---|---|---|
| Van der Waal energy | $-88.632 \pm$ 14.668 | $-107.106 \pm$ 16.147 | $-121.404 \pm 15.007$ |
| Electrostatic energy | $-13.698 \pm$ 10.616 | $-23.926 \pm$ 13.358 | $-18.129 \pm 13.102$ |
| Polar solvation energy | $73.315 \pm$ 14.088 | $104.600 \pm$ 19.421 | $82.270 \pm 16.855$ |
| SASA energy | $-11.446 \pm$ 1.322 | $-13.025 \pm$ 1.269 | $-13.543 \pm 1.276$ |
| Binding energy | $-40.461 \pm$ 10.567 | $-39.457 \pm$ 14.198 | $-70.807 \pm 13.517$ |

acacetin. Table 7 shows the mean values of RMSD, Rg, SASA, and average hydrogen bond number of various systems, along with their standard deviations.

The essential dynamic behaviour of the 6LU7- acacetin, 6Y2E-acacetin and spike RBD-acacetin was studied by using the modules *gmxcovar and gmxanaeig*. Principal component analysis was studied correlated motions of the above models.Covariance matrix diagonalization was used to verify the flexible aspect. Fig. 18 depicts the obtained eigen values and eigen vectors as a consequence of this matrix. This finding contains information about the correlated motions. The flexibility of all the structures, including 6LU7- acacetin and 6Y2E-acacetin, can be seen in the trace value of this matrix. 6LU7- acacetin, 6Y2E-acacetin and spike RBD-acacetin have values of 12.29, 6.27 and 10.33 nm², respectively. The lower value of covariance matrix of 6Y2E-acacetin (6.27 nm²) leads to the less dynamic structural conformation of the complex as compared to 6LU7- acacetin and spike RBD-acacetin.

To elucidate the sub conformational patterns of 6LU7-acacetin,6Y2E-acacetin and spike RBD-acacetin complexes, we studied the free energy landscape [70,71] against first two principal components PC1 and PC2. The free energy landscape of 6LU7-acacetin,6Y2E-acacetin and spike RBD-acacetin system was shown in Fig. 19. The size and shape of the minimum energy region (in violet color) indicates a complex's stability. Spike RBD-acacetin complex have several minima. Both 6LU7- acacetin and 6Y2E-acacetin complex achieved single energy minima. From MM-PBSA results revealed that, acacetin acts as good inhibitor towards main protease. Graphical representation of Van der Waals energy, electrostatic energy and binding energy of 6LU7-acacetin, 6Y2E-acacetin systems and Spike RBD-acacetin system were shown in Fig. 20. Table 8 displays the different energies obtained from the MM-PBSA method for the 6LU7-acacetin, 6Y2E-acacetin systems and spike RBD - acacetin system.

## 4. Summary and conclusion

In this study, we have screened 12 major bioactive compounds out of 424 compounds obtained from herbal solution through GCMS analysis. The binding affinity as well as physicochemical properties of the thebaine, acacetin, indomethacin, crinamineacetate,(S)-1-Piperideine-6-carboxylate, levamisole, melatonin, nicotinic acid, curcumin, methotrimeprazine, omeprazole, and methaqualone phytocompounds with main protease proteins as well as with mutant (at position L452R and E484Q) of receptor binding domain of spike protein were analyzed through molecular docking study. Finally, 100 ns molecular dynamics simulations were used to examine their dynamic properties as well as conformational flexibility and stability.LEU50, ASN72, PRO96, Tyr 154, GLY170, ALA 193, ARG 222, and MET 274 residues of main protease play a crucial role in binding with ligands. The present study revealed a noticeable interaction of GLY446, SER477, GLY482, THR500 and

LEU518 residues with mutant of receptor binding domain of spike protein. LEU50, ASN72, PRO96, TYR154, GLY170, ARG222, and MET274 residues of main protease play a crucial role in binding with ligands. The present study revealed a noticeable interaction of GLY446, SER477, GLY482, THR500 and LEU518 residues with mutant of spike receptor binding domain protein were observed. From MM-PBSA results it was observed that, acacetin acts as good inhibitor towards main protease. From molecular docking study and molecular dynamics study revealed that, the compound acacetin shows promising inhibitor towards both main protease as well as mutant spike RBD of SARS-CoV-2 protein.

## Declaration of competing interest

We declared that we have no conflict.

## Acknowledgements

## Appendix A. Supplementary data

Supplementary data to this article can be found online at https://doi.org/10.1016/j.jics.2022.100417.

## References

[1] M. Qasim, Y. Fujii, M.Z. Ahmed, I. Aziz, K.N. Watanabe, M. Ajmal Khan, Phytotoxic analysis of coastal medicinal plants and quantification of phenolic compounds using HPLC, Plant Biosyst.Int. J. Deal.Aspects.Plant Biol. 153 (6) (2019) 767–774.
[2] K.S. Rao, R. Hariharan, V.S. Rajpoot, Ethnobotanical survey of folk medicinal plants used in tribal villages of Amarkantak Region of Central India, Plant Biosyst. Int. J. Deal.Aspects.Plant Biol. (2021) 1–61 (just-accepted).
[3] A.M. Saab, M. Tacchini, G. Sacchetti, C. Contini, H. Schulz, I. Lampronti, G. Racagni, Phytochemical analysis and potential natural compounds against SARS-CoV-2/COVID-19 in essential oils derived from medicinal plants originating from Lebanon. An information note, Plant Biosyst.Int. J. Deal.Aspects.Plant Biol. (2021) 1–17 (just-accepted).
[4] M. Bonesi, A.M. Saab, M.C. Tenuta, M. Leporini, M.J. Saab, M.R. Loizzo, R. Tundis, Screening of traditional Lebanese medicinal plants as antioxidants and inhibitors of key enzymes linked to type 2 diabetes, Plant Biosyst.Int. J. Deal.Aspects.Plant Biol. 154 (5) (2020) 656–662.
[5] H. R Vasanthi, N. ShriShriMal, D. K Das, Phytochemicals from plants to combat cardiovascular disease, Curr. Med. Chem. 19 (14) (2012) 2242–2251.
[6] M.H. Baig, A.T. Jan, G. Rabbani, K. Ahmad, J.M. Ashraf, T. Kim, I. Choi, Methylglyoxal and Advanced Glycation End products: insight of the regulatory machinery affecting the myogenic program and of its modulation by natural compounds, Sci. Rep. 7 (1) (2017) 1–10.
[7] Y. Yang, M.S. Islam, J. Wang, Y. Li, X. Chen, Traditional Chinese medicine in the treatment of patients infected with 2019-new coronavirus (SARS-CoV-2): a review and perspective, Int. J. Biol. Sci. 16 (10) (2020) 1708.
[8] S. Khaerunnisa, H. Kurniawan, R. Awaluddin, S. Suhartati, S. Soetjipto, Potential Inhibitor of COVID-19 Main Protease (Mpro) from Several Medicinal Plant Compounds by Molecular Docking Study, Prepr. doi10.2020, pp. 1–14, 20944.
[9] V.K. Maurya, S. Kumar, A.K. Prasad, M.L. Bhatt, S.K. Saxena, Structure-based Drug Designing for Potential Antiviral Activity of Selected Natural Products from Ayurveda against SARS-CoV-2 Spike Glycoprotein and its Cellular Receptor, 2020, pp. 1–15, VirusDisease.
[10] A. Rakib, A. Paul, M. Chy, N. Uddin, S.A. Sami, S.K. Baral, M. Majumder, A. M. Tareq, M.N. Amin, A. Shahriar, M. Uddin, Biochemical and computational approach of selected phytocompounds from tinosporacrispa in the management of COVID-19, Molecules 25 (17) (2020) 3936.
[11] Z.T. Muhseen, A.R. Hameed, H.M. Al-Hasani, M.T. ul Qamar, G. Li, Promising terpenes as SARS-CoV-2 spike receptor-binding domain (RBD) attachment inhibitors to the human ACE2 receptor: integrated computational approach, J. Mol. Liq. 320 (2020) 114493.
[12] A. Sharma, S. Goyal, A.K. Yadav, P. Kumar, L. Gupta, In-silico screening of plant-derived antivirals against main protease, 3CLpro and endoribonuclease, NSP15 proteins of SARS-CoV-2, J. Biomol. Struct. Dyn. (2020) 1–15.
[13] F. Shifah, A.M. Tareq, M.A. Sayeed, M.N. Islam, T.B. Emran, M.A. Ullah, M. A. Mukit, A. Ullah, Antidiarrheal, cytotoxic and thrombolytic activities of methanolic extract of Hedychium coccineum leaves, measurement 11 (2020) 12.
[14] A.M. Tareq, S. Farhad, A.N. Uddin, M. Hoque, M.S. Nasrin, M.M.R. Uddin, M. Hasan, A. Sultana, M.S. Munira, C. Lyzu, S.M. Hossen, Chemical profiles,

[15] pharmacological properties, and in silico studies provide new insights on Cycas pectinata, Heliyon 6 (6) (2020) e04061.
[15] F. Wu, S. Zhao, B. Yu, Y.M. Chen, W. Wang, Z.G. Song, Y. Hu, Z.W. Tao, J.H. Tian, Y.Y. Pei, M.L. Yuan, A new coronavirus associated with human respiratory disease in China, Nature 579 (7798) (2020) 265–269.
[16] C.C. Lai, T.P. Shih, W.C. Ko, H.J. Tang, P.R. Hsueh, Severe acute respiratory syndrome coronavirus 2 (SARS-CoV-2) and corona virus disease-2019 (COVID-19): the epidemic and the challenges, Int. J. Antimicrob. Agents (2020) 105924.
[17] A.M. Zaki, S. Van Boheemen, T.M. Bestebroer, A.D. Osterhaus, R.A. Fouchier, Isolation of a novel coronavirus from a man with pneumonia in Saudi Arabia, N. Engl. J. Med. 367 (19) (2012) 1814–1820.
[18] M.A. Zamzami, G. Rabbani, A. Ahmad, A.A. Basalah, W.H. Al-Sabban, S.N. Ahn, H. Choudhry, Carbon nanotube field-effect transistor (CNT-FET)-based biosensor for rapid detection of SARS-CoV-2 (COVID-19) surface spike protein S1, Bioelectrochemistry 143 (2022) 107982.
[19] D. Wrapp, N. Wang, K.S. Corbett, J.A. Goldsmith, C.L. Hsieh, O. Abiona, B. S. Graham, J.S. McLellan, Cryo-EM structure of the 2019-nCoV spike in the prefusion conformation, Science 367 (6483) (2020) 1260–1263.
[20] H.M. Mengist, X. Fan, T. Jin, Designing of improved drugs for COVID-19: crystal structure of SARS-CoV-2 main protease M pro, Signal Transduct.Targeted.Ther. 5 (1) (2020) 1–2.
[21] Z. Ren, L. Yan, N. Zhang, Y. Guo, C. Yang, Z. Lou, Z. Rao, The newly emerged SARS-like coronavirus HCoV-EMC also has an" Achilles' heel": current effective inhibitor targeting a 3C-like protease, Protein & cell 4 (4) (2013) 248.
[22] H. Zhang, J.M. Penninger, Y. Li, N. Zhong, A.S. Slutsky, Angiotensin-converting enzyme 2 (ACE2) as a SARS-CoV-2 receptor: molecular mechanisms and potential therapeutic target, Intensive Care Med. 46 (4) (2020) 586–590.
[23] X. Liu, B. Zhang, Z. Jin, H. Yang, Z. Rao, RCSB Protein Data Bank, 2020.
[24] Q.S. Du, S.Q. Wang, Y. Zhu, D.Q. Wei, H. Guo, S. Sirois, K.C. Chou, Polyprotein cleavage mechanism of SARS CoVMpro and chemical modification of the octapeptide, Peptides 25 (11) (2004) 1857–1864.
[25] W. Dai, B. Zhang, X.M. Jiang, H. Su, J. Li, Y. Zhao, X. Xie, Z. Jin, J. Peng, F. Liu, C. Li, Structure-based design of antiviral drug candidates targeting the SARS-CoV-2 main protease, Science 368 (6497) (2020) 1331–1335.
[26] A. El Alami, A. Fattah, A. Chait, Medicinal plants used for the prevention purposes during the covid-19 pandemic in Morocco, J.Anal. Sci.Appl. Biotechnol. 2 (1) (2020), 2-1.
[27] D.E. Gordon, G.M. Jang, M. Bouhaddou, J. Xu, K. Obernier, K.M. White, M. J. O'Meara, V.V. Rezelj, J.Z. Guo, D.L. Swaney, T.A. Tummino, A SARS-CoV-2 protein interaction map reveals targets for drug repurposing, Nature (2020) 1–13.
[28] J. Cho, Y.J. Lee, J.H. Kim, S. il Kim, S.S. Kim, B.S. Choi, J.H. Choi, Antiviral activity of digoxin and ouabain against SARS-CoV-2 infection and its implication for COVID-19, Sci. Rep. 10 (1) (2020) 1–8.
[29] G. Rabbani, S.N. Ahn, Roles of human serum albumin in prediction, diagnoses and treatment of COVID-19, Int. J. Biol. Macromol. 193 (2021) 948–955.
[30] L. Zhang, D. Lin, X. Sun, U. Curth, C. Drosten, L. Sauerhering, S. Becker, K. Rox, R. Hilgenfeld, Crystal structure of SARS-CoV-2 main protease provides a basis for design of improved α-ketoamide inhibitors, Science 368 (6489) (2020) 409–412.
[31] Q. Wang, Y. Zhang, L. Wu, S. Niu, C. Song, Z. Zhang, J. Qi, Structural and functional basis of SARS-CoV-2 entry by using human ACE2, Cell 181 (4) (2020) 894–904.
[32] Q. Li, J. Wu, J. Nie, L. Zhang, H. Hao, S. Liu, Y. Wang, The impact of mutations in SARS-CoV-2 spike on viral infectivity and antigenicity, Cell 182 (5) (2020) 1284–1294.
[33] N. Kaushal, Y. Gupta, M. Goyal, S.F. Khaiboullina, M. Baranwal, S.C. Verma, Mutational frequencies of SARS-CoV-2 genome during the beginning months of the outbreak in USA, Pathogens 9 (7) (2020) 565.
[34] B. Korber, W.M. Fischer, S. Gnanakaran, H. Yoon, J. Theiler, W. Abfalterer, D. C. Montefiori, Tracking changes in SARS-CoV-2 spike: evidence that D614G increases infectivity of the COVID-19 virus, Cell 182 (4) (2020) 812–827.
[35] L. Guruprasad, Human SARS CoV-2 spike protein mutations, Proteins: Structure, Function, and Bioinformatics 89 (5) (2021) 569–576.
[36] G. Rabbani, S.N. Ahn, H. Kwon, K. Ahmad, I. Choi, Penta-peptide ATN-161 based neutralization mechanism of SARS-CoV-2 spike protein, Biochem. Biophys.Reports 28 (2021) 101170.
[37] S. Cherian, V. Potdar, S. Jadhav, P. Yadav, N. Gupta, M. Das, P. Rakshit, S. Singh, P. Abraham, S. Panda, N.I.C. Team, SARS-CoV-2 spike mutations, L452R, T478K, E484Q and P681R, in the second wave of COVID-19 in Maharashtra, India, Microorganisms 9 (7) (2021) 1542.
[38] M. Verghese, B. Jiang, N. Iwai, M. Mar, M.K. Sahoo, F. Yamamoto, B.A. Pinsky, Identification of a SARS-CoV-2 variant with L452R and E484Q neutralization resistance mutations, J. Clin. Microbiol. 59 (7) (2021) e00741–21.
[39] O. Trott, A.J. Olson, AutoDock Vina: improving the speed and accuracy of docking with a new scoring function, efficient optimization, and multithreading, J. Comput. Chem. 31 (2) (2010) 455–461.
[40] G. Rabbani, E.J. Lee, K. Ahmad, M.H. Baig, I. Choi, Binding of tolperisone hydrochloride with human serum albumin: effects on the conformation, thermodynamics, and activity of HSA, Mol. Pharm. 15 (4) (2018) 1445–1456.
[41] G. Rabbani, M.H. Baig, A.T. Jan, E.J. Lee, M.V. Khan, M. Zaman, I. Choi, Binding of erucic acid with human serum albumin using a spectroscopic and molecular docking study, Int. J. Biol. Macromol. 105 (2017) 1572–1580.
[42] G. Rabbani, M.H. Baig, E.J. Lee, W.K. Cho, J.Y. Ma, I. Choi, Biophysical study on the interaction between eperisone hydrochloride and human serum albumin using spectroscopic, calorimetric, and molecular docking analyses, Mol. Pharm. 14 (5) (2017) 1656–1665.
[43] D.S. Visualizer, Version 2.0. 1.7347, Accelrys Software Inc., San Diego, 2013.

[44] A. Daina, O. Michielin, V. Zoete, SwissADME: a free web tool to evaluate pharmacokinetics, drug-likeness and medicinal chemistry friendliness of small molecules, Sci. Rep. 7 (2017) 42717.

[45] S.K. Pattanayak, S. Chowdhuri, Effect of water on solvation structure and dynamics of ions in the peptide bond environment: importance of hydrogen bonding and dynamics of the solvents, J. Phys. Chem. B 115 (45) (2011) 13241–13252.

[46] S.K. Pattanayak, S. Chowdhuri, Effects of concentrated NaCl and KCl solutions on the behaviour of aqueous peptide bond environment: single-particle dynamics and H-bond structural relaxation, Mol. Phys. 111 (21) (2013) 3297–3310.

[47] S.K. Pattanayak, P. Chettiyankandy, S. Chowdhuri, Effects of co-solutes on the hydrogen bonding structure and dynamics in aqueous N-methylacetamide solution: a molecular dynamics simulations study, Mol. Phys. 112 (22) (2014) 2906–2919.

[48] D. Van Der Spoel, E. Lindahl, B. Hess, G. Groenhof, A.E. Mark, H.J. Berendsen, GROMACS: fast, flexible, and free, J. Comput. Chem. 26 (16) (2005) 1701–1718.

[49] K. Vanommeslaeghe, A.D. MacKerell Jr., Automation of the CHARMM General Force Field (CGenFF) I: bond perception and atom typing, J. Chem. Inf. Model. 52 (12) (2012) 3144–3154.

[50] J. Huang, S. Rauscher, G. Nawrocki, T. Ran, M. Feig, B.L. de Groot, H. Grubmüller, A.D. MacKerell, CHARMM36: an improved force field for folded and intrinsically disordered proteins, Biophys. J. 112 (3) (2017) 175a–176a.

[51] Y. Sun, P.A. Kollman, Hydrophobic solvation of methane and nonbond parameters of the TIP3P water model, J. Comput. Chem. 16 (9) (1995) 1164–1169.

[52] R. Fletcher, M.J. Powell, A rapidly convergent descent method for minimization, Comput. J. 6 (2) (1963) 163–168.

[53] H.J.C. Berendsen, J.P.M. Postma, W.F. Van Gunsteren, A. Dinola, J.R. Haak, Molecular dynamics with coupling to an external bath, J. Chem. Phys. 81 (8) (1984) 3684–3690.

[54] M. Parrinello, A. Rahman, Crystal structure and pair potentials: a molecular-dynamics study, Phys. Rev. Lett. 45 (14) (1980) 1196–1199.

[55] B. Hess, H. Bekker, H.J. Berendsen, J.G. Fraaije, LINCS: a linear constraint solver for molecular simulations, J. Comput. Chem. 18 (12) (1997) 1463–1472.

[56] P.P. Ewald, Die Berechnungoptischer und elektrostatischerGitterpotentiale, Ann. Phys. 369 (3) (1921) 253–287.

[57] V.K. Maurya, S. Kumar, M.L. Bhatt, S.K. Saxena, Antiviral activity of traditional medicinal plants from Ayurveda against SARS-CoV-2 infection, J. Biomol. Struct. Dyn. (2020) 1–17.

[58] B. Adhikari, B.P. Marasini, B. Rayamajhee, B.R. Bhattarai, G. Lamichhane, K. Khadayat, A. Adhikari, S. Khanal, N. Parajuli, Potential Roles of Medicinal Plants for the Treatment of Viral Diseases Focusing on COVID-19: A Review, Phytotherapy Research, 2020.

[59] M.A. Marinella, Indomethacin and resveratrol as potential treatment adjuncts for SARS-CoV-2/COVID-19, Int. J. Clin. Pract. (2020) e13535.

[60] P. Khumkhrong, K. Piboonprai, W. Chaichompoo, W. Pimtong, M. Khongkow, K. Namdee, A. Jantimaporn, D. Japrung, U. Asawapirom, A. Suksamrarn, T. Iempridee, Crinamine induces apoptosis and inhibits proliferation, migration, and angiogenesis in cervical cancer SiHaCells, Biomolecules 9 (9) (2019) 494.

[61] R. Singh, T. Arif, I. Khan, P. Sharma, Phytochemicals in antidiabetic drug discovery, J Biomed Ther Sci 1 (2014) 1–33.

[62] R.F. Liu, C.B. Chen, R.C. Hui, Y.Z. Kuan, W.H. Chung, The effect of levamisole in the treatment of recalcitrant recurrent erythema multiforme major: an observational study, J. Dermatol. Sci. 92 (1) (2018) 38–44.

[63] E.L. Feitosa, F.T.D.S. Júnior, J.A.D.O.N. Neto, L.F. Matos, M.H.D.S. Moura, T. O. Rosales, G.B.L. De Freitas, COVID-19: rational discovery of the therapeutic potential of Melatonin as a SARS-CoV-2 main Protease Inhibitor, Int. J. Med. Sci. 17 (14) (2020) 2133.

[64] C. Gaudineau, R. Beckerman, S. Welbourn, K. Auclair, Inhibition of human P450 enzymes by multiple constituents of the Ginkgo biloba extract, Biochem. Biophys. Res. Commun. 318 (4) (2004) 1072–1078.

[65] Y. Manoharan, V. Haridas, K.C. Vasanthakumar, S. Muthu, F.F. Thavoorullah, P. Shetty, Curcumin: a wonder drug as a preventive measure for COVID19 management, Indian J. Clin. Biochem. 35 (3) (2020) 373–375.

[66] D.K. Arya, A. Verma, D. Singh, J.B.S. Kachhawa, A Review on Pharmacological/ biological Activities of Different Derivatives of Phenothiazines, vol. 2, 2013, pp. 24–31, 02.

[67] O.S. Oladeji, F.E. Adelowo, A.P. Oluyori, D.T. Bankole, Ethnobotanical Description and Biological Activities of Senna alata, Evidence-Based Complementary and Alternative Medicine, 2020, 2020.

[68] S.N. Sahu, S.K. Pattanayak, Molecular docking and molecular dynamics simulation studies on PLCE1 encoded protein, J. Mol. Struct. 1198 (2019) 126936.

[69] S.N. Sahu, M. Moharana, R. Sahu, S.K. Pattanayak, Impact of mutation on podocin protein involved in type 2 nephrotic syndrome: insights into docking and molecular dynamics simulation study, J. Mol. Liq. 281 (2019) 549–562.

[70] S.N. Sahu, B. Mishra, R. Sahu, S.K. Pattanayak, Molecular dynamics simulation perception study of the binding affinity performance for main protease of SARS-CoV-2, J. Biomol. Struct. Dyn. (2020) 1–16.

[71] S.N. Sahu, S.S. Satpathy, C. Mohanty, S.K. Pattanayak, Computational study to evaluate the potency of phytochemicals in Boerhavia diffusa and the impact of point mutation on cyclin-dependent kinase 2-associated protein 1, J. Biomol. Struct. Dyn. (2021) 1–15.